

18th Australian International Aerospace Congress 27th International Symposium on Space Flight Dynamics

Please select category below:

Normal Paper

Student Paper

Young Engineer Paper

Enhancement of the Spacecraft Attitude Dynamics Capabilities via Combination of the Inertial Morphing and Reaction Wheels (*Keynote Paper and Presentation*)

Pavel M. Trivailo¹ and Hirohisa Kojima³

¹ RMIT University, School of Engineering, GPO Box 2476V, Melbourne, Victoria, 3001, Australia, pavel.trivailo@rmit.edu.au

² Tokyo Metropolitan University, Department of Aeronautics and Astronautics, Asahigaoka 6-6, Hino, Tokyo, Japan, 191-0065, hkojima@tmu.ac.jp

Abstract

In our previous works [1-4] we discovered an efficient method of control of the inversion of the spinning spacecraft. This method was prompted by the “Dzhanibekov’s Effect” or “Tennis Racket Theorem” [4], which are often seen by many as odd or even mysterious. The proposed spacecraft inversion method does not employ conventional RWs, but, instead, is using proposed morphing of the inertial properties of the spinning spacecraft. It allows to completely stop flipping motion or activate flipping motion on the spacecraft, being in its stable spin.

In this paper, we are considering a spacecraft, which has both, inertial morphing and RW, capabilities. It is believed that performance of the RW systems could be enhanced with the inertial morphing. For general formulation, we first assume ability of the spacecraft to change its inertial properties, associated with all three principal axes of inertia. Secondly, we also assume that the spacecraft is equipped with three control wheels, located along the x , y and z -axes of the body-fixed frame. For simulation of these types of spacecraft systems, extended Euler’s equations are used and peculiar dynamics of the spacecraft is illustrated with a several study cases. We illustrate complex spacecraft attitude dynamics manoeuvres, using geometric interpretation, employing angular momentum spheres and kinetic energy ellipsoids. We demonstrate individual and aggregated contributions of the inertial morphing and RW to the changes of the shape of the kinetic energy ellipsoid and relate this to the resultant various feature manoeuvres, including inversion and re-orientation. We discuss enhancements of each of the control capabilities, morphing and RW. For the periodic inversion motions, we perform calculation of the periods of the flipping motion, based on the complete elliptic integral of the first kind and present in a systematic way flipping periods for various combinations of inertial properties of the spacecraft. We discuss strategies leading to the increase or reduction of the flipping and/or wobbling motions. A discovered “asymmetric ridge” of high periods for peculiar combinations of the inertial properties is discussed in detail. Numerous examples are illustrated with animations in Virtual Reality, facilitating explanation of the analysis and control methodologies to a wide audience, including specialists, industry and students.

Keywords: spacecraft attitude dynamics, Euler’s equations of motion, morphing spacecraft, reaction wheel (RW), angular momentum sphere, kinetic energy ellipsoid, flipping period.

Introduction

The paper is aiming to contribute to the attitude dynamics and control of spacecraft and was prompted by an interesting phenomenon, known as “Dzhanibekov’s Effect” and “Tennis Racquet Theorem” [5]. Developing numerical simulation tools and analysis to explore these phenomenon and its geometric interpretation, it was possible to discover a new concept of the “inertial morphing” of the spacecraft systems to effectively control the “Dzhanibekov’s Effect”, presented in our recent works [1-4] and extend it further to enable attitude control of the spinning/tumbling systems, converting compound motions into simple spins about one of the selected/nominated body axes.

Leonard Euler and his Famous Equations for the Rigid Body Dynamics

Leonhard Euler (April 15, 1707 - Sept. 18, 1783) was a famous Swiss physicist and mathematician (the most eminent of the 18th century and one of the greatest in history), who made key contributions to various fields of mathematics and mechanics, leaving long-lasting heritage of more than 500 books and papers. (His portrait is presented in Fig. 1a).

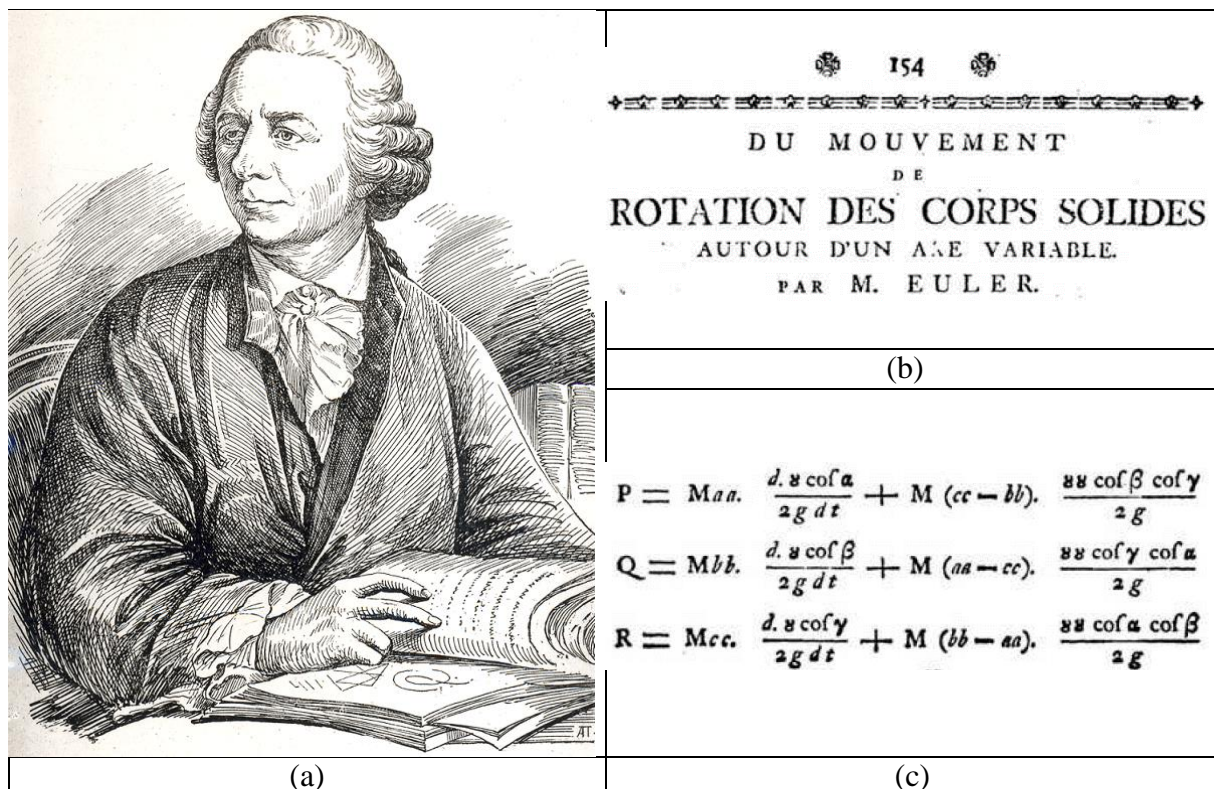


Fig. 1: (a) Leonard Euler’s portrait from the University of Tartu collection [6].
 (b) The title of the historic Leonard Euler’s work [7], dated by 1758.
 (c) Euler’s equations as they appeared in the original L.Euler’s work [8].

It has been computed that his publications during his working life averaged about 800 pages a year. Euler was one of the most eminent mathematicians of the 18th century, and is held to be one of the greatest in history. His “Euler’s identity” is considered an example of mathematical beauty:

$$e^{i\pi} + 1 = 0 \quad (1)$$

called "the most remarkable formula in mathematics" by Richard P. Feynman [9], for its single uses of the notions of addition, multiplication, exponentiation, and equality, and the single uses of the important constants 0, 1, e , i and π .

In 1988, readers of the Mathematical Intelligencer voted it "the Most Beautiful Mathematical Formula Ever". In total, Euler was responsible for three of the top five formulae in that poll [10]. His interests are amazingly versatile. Even when dealing with music, Euler's approach is mainly mathematical. His writings on music are not particularly numerous (a few hundred pages, in his total production of about thirty thousand pages), but they reflect an early preoccupation and one that did not leave him throughout his life.

Among numerous Euler's works, he developed rigid-body dynamics, very influential publication has a very special place in history. It presented Euler's equations for the dynamics of a rigid body, widely used in modern engineering and science.

Being always fascinated with Euler's scientific work and heritage, the authors were delighted to find in the Euler's archive his original work. It is with greatest pleasure and a profound sense of tribute to Great Euler, we are reproducing famous Euler's equations, exactly as they appeared in Euler's original work.

In Fig. 1c we show the title of the publication, available from the Euler's archive [8] and the Euler equations.

Euler's Dynamic Equations for the Motion of a Rigid Body

The iconic Euler dynamic equations of motion of the rigid body with constant values of the principal moments of inertia, can be written as [7, 11]:

$$\begin{cases} I_{xx} \dot{\omega}_x = (I_{yy} - I_{zz}) \omega_y \omega_z \\ I_{yy} \dot{\omega}_y = (I_{zz} - I_{xx}) \omega_z \omega_x \\ I_{zz} \dot{\omega}_z = (I_{xx} - I_{yy}) \omega_x \omega_y \end{cases} \quad (2)$$

These differential equations could be easily solved numerically, if particular initial conditions are specified. One of the possible techniques is based on the Runge-Kutta methods, implemented in MATLAB and Cleve Moler, founder of Mathworks, provides with an amazing interactive tools implementing this strategy [12]. Another possibility is to re-write Eqs.(2) in terms of the quaternions and solve these resultant equations.

Non-Dimensional Formulation of the Equations

For the main derivations in this paper we will typically assume that the system has *three distinct* principal moments of inertia, which are *arranged* in the following order: $I_{xx} < I_{yy} < I_{zz}$. For more generic formulations, let us introduce two non-dimensional parameters, η and ξ , both restricted in their values within the range between 0 and 1:

$$\eta = \frac{I_{xx}}{I_{zz}}; \quad \xi = \frac{I_{yy} - I_{xx}}{I_{zz} - I_{xx}}; \quad (0 < \eta < 1; \quad 0 < \xi < 1) \quad (3)$$

Parameter ξ in this case would have a similar meaning of the non-dimensional coordinate "counterpart" from the Finite Element Method, defining the current position within the finite element. In the context of our study, ξ is specifying the non-dimensional relative position coordinate of the intermediate value of the moment of inertia between the minimum value of the moment of inertia I_{xx} and the maximum value of the moment of inertia I_{zz} . In other words, it can be said that ξ is the non-dimensional parameter in the Hermite functions, enabling calculation of I_{yy} using I_{xx} and I_{zz} , using the following relationship:

$$I_{yy} = I_{xx} (1 - \xi) + I_{zz} \xi \quad (4)$$

Zero value of ξ would now correspond to I_{xx} and unit value of ξ would correspond to I_{zz} and any intermediate value of ξ , expressed via $0 < \xi < 1$, would correspond to I_{yy} . With these notations, we can also derive several relationships, enabling useful conversions in the future:

$$I_{yy} = I_{xx} \left(1 - \xi + \frac{1}{\eta} \right); \quad I_{zz} = \frac{I_{xx}}{\eta}; \quad \xi = \frac{I_{yy} - I_{xx}}{I_{zz} - I_{xx}} \quad (5)$$

For illustration purposes, we solve Euler's Eqs.(2) for the same system with $I_{yy} = 2$; $I_{yy} = 3$; $I_{yy} = 4$ [all in $\text{kg}\cdot\text{m}^2$], which correspond to $\xi = 0.5$ and $\eta = 0.5$, but consider three contrast cases of the initial conditions. Results of the numerical simulations for $\omega_x, \omega_y, \omega_z$ are shown in Fig.2.

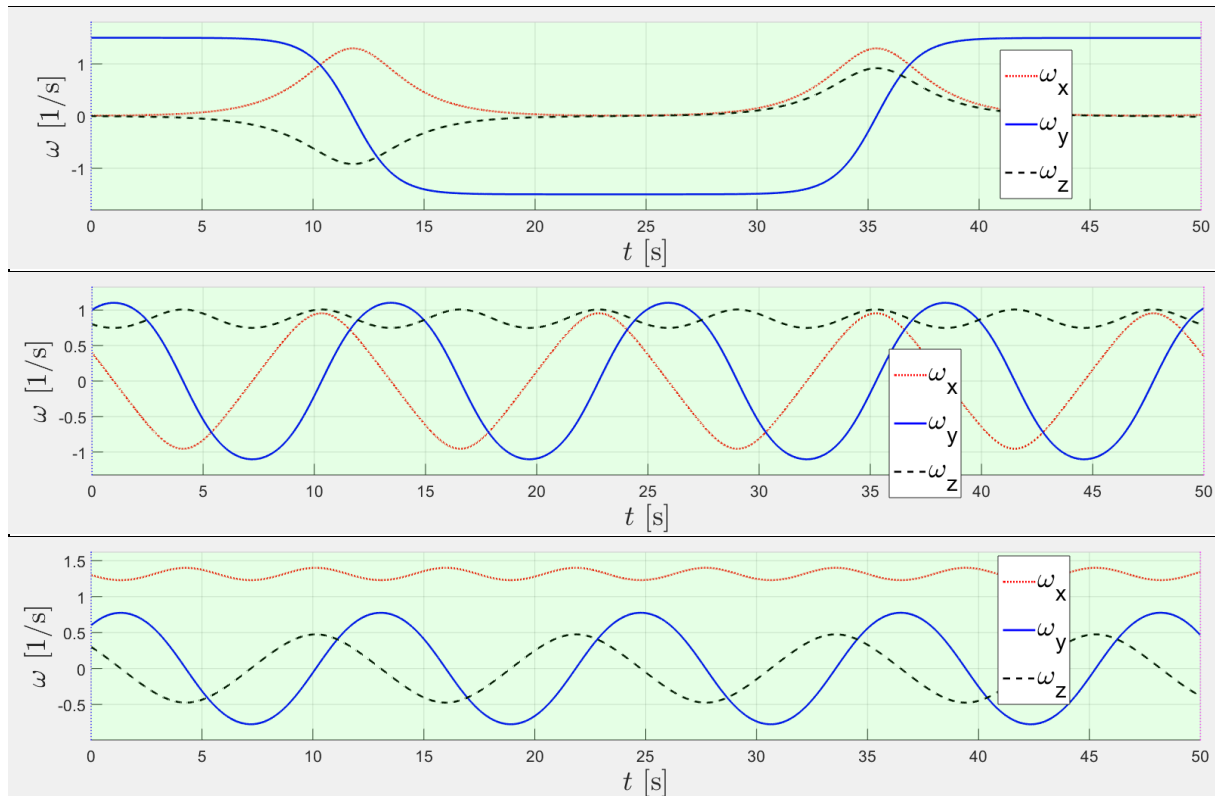


Fig.2: Time histories for angular velocity components $\omega_x, \omega_y, \omega_z$ for three contrast cases of initial conditions: (A) $\omega_{x0}=0.01, \omega_{y0}=1.5, \omega_{z0}=0$; (B) $\omega_{x0}=0.4, \omega_{y0}=1, \omega_{z0}=0.8$; (C) $\omega_{x0}=1.3, \omega_{y0}=0.6, \omega_{z0}=0.3$ (here and further all angular velocities are given in rad/s).

For more general interpretation, we are proposing to introduce non-dimensional angular momentum coordinates:

$$\begin{aligned} \bar{H}_x(t) &= H_x / H_0 = I_{xx} \omega_x / \sqrt{(I_{xx} \omega_x)^2 + (I_{yy} \omega_y)^2 + (I_{zz} \omega_z)^2} \\ \bar{H}_y(t) &= H_y / H_0 = I_{yy} \omega_y / \sqrt{(I_{xx} \omega_x)^2 + (I_{yy} \omega_y)^2 + (I_{zz} \omega_z)^2} \\ \bar{H}_z(t) &= H_z / H_0 = I_{zz} \omega_z / \sqrt{(I_{xx} \omega_x)^2 + (I_{yy} \omega_y)^2 + (I_{zz} \omega_z)^2} \end{aligned} \quad (6)$$

and show results in the $\bar{H}_x, \bar{H}_y, \bar{H}_z$ coordinates. Fig.3 shows previous cases A, B and C as trajectories (shown with red color) of the tip of the non-dimensional angular momentum vector, $\bar{\mathbf{H}}$, called polhodes [11]. Fig.3 also shows superimposed three quiver plots for $\bar{\mathbf{H}}$ vectors.

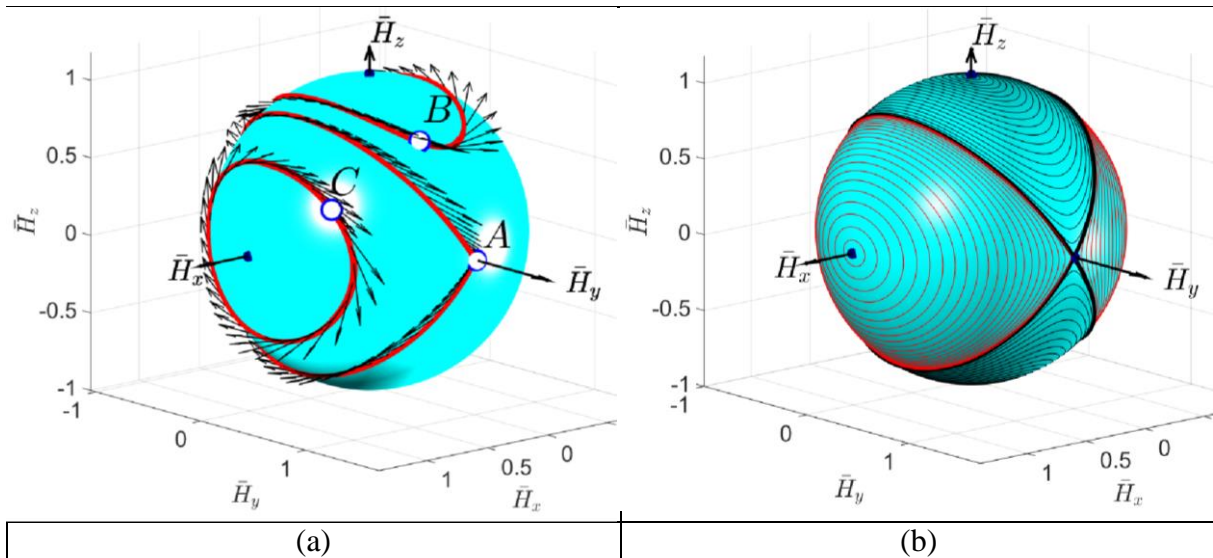


Fig.3: Polhodes: (a) for demo cases A, B and C in Fig.2; (b) examples of broad coverage of initial conditions.

Polhodes and Separatrices

Fig.3b shows that the polhodes can be split into four groups, separated by the (shown as bold black) lines, called separatrices. In case of I_{yy} being the intermediate moment of inertia, two separatrics intersect at the points on the y axis. It is possible to show that polhodes are seen on orthogonal projections as ellipses, hyperbolas and ellipses and separatrics are seen on the x - z projection as two lines, passing through the y axis, reduced on projection to a dot. We can calculate a very important characteristic of the rotational motion of the spacecraft, α - angle of inclination of the separatrix plane with respect to the z axis [2]:

$$\alpha = \arctan \left(\sqrt{\frac{I_x(I_y - I_z)}{I_z(I_x - I_y)}} \right) = \arctan \left(\sqrt{\eta \left(\frac{1}{\xi} - 1 \right)} \right) \quad (7)$$

(only applicable for the $I_{xx} < I_{yy} < I_{zz}$ notations and $0 < \eta < 1$ and $0 < \xi < 1$)

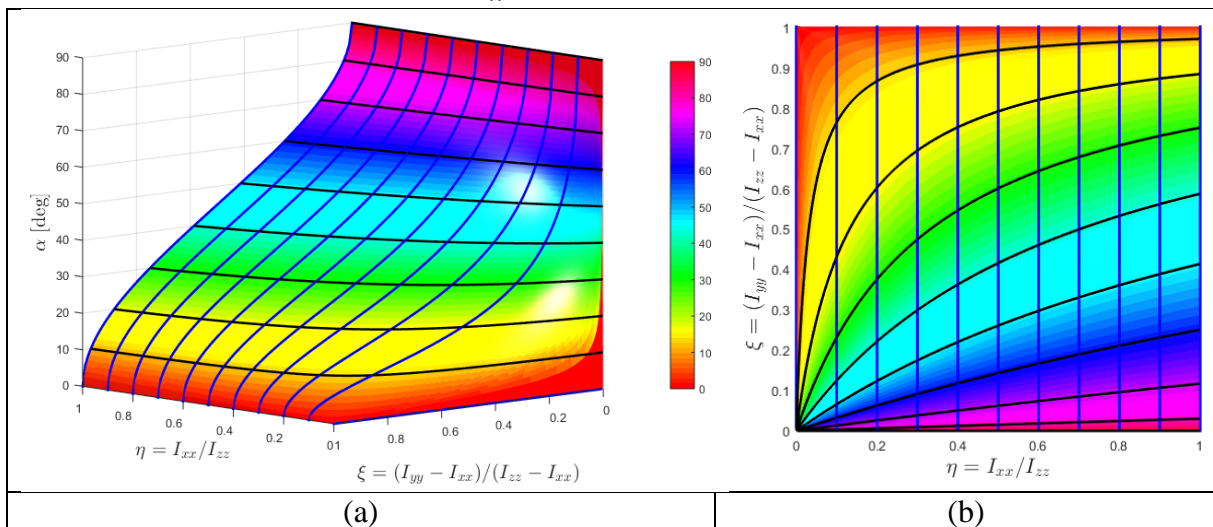


Fig.4: Changes in the angle α due to the variation in both, η and ξ :

(a) 3D surface plot for $\alpha(\eta, \xi)$ function with colorbar added;

(b) 2D projection of the $\alpha(\eta, \xi)$ surface with its contour lines: $\eta = 0:0.1:1$; $\alpha = 0:10:90$.

Changes in the angle α due to the variation in both, η and ξ , are shown in Fig.4. Note, that for convenience, values of α angles are presented in degrees.

The method, described in [2], was based on the calculation of the value of the intermediate moment of inertia I_{yy} for the specified angle α and known values of $I_{xx}=2.4$ and $I_{zz}=3.15$. For this formulation, Eq.(7) can be re-written as follows:

$$\xi = \left\{ 1 + \left[(\tan \alpha)^2 / \eta \right] \right\}^{-1} \quad (8)$$

For the particular case, considered in [2], for $I_{xx}=2.4$ and $I_{zz}=3.15$, the corresponding value of η is equal to $\eta=0.7619$; furthermore, Eq.(8) gives $\xi=0.5907$, which (as per Eq. (3)), corresponds to $I_{xx}= 2.8430$.

The generic graphical method, corresponding to this procedure, is illustrated in Fig.5, where angle α (shown in degrees) is plotted as a function of ξ for various values of $\eta=[.1, .2, .3, .4, .5, .6, .7, .8, .9, 1]$.

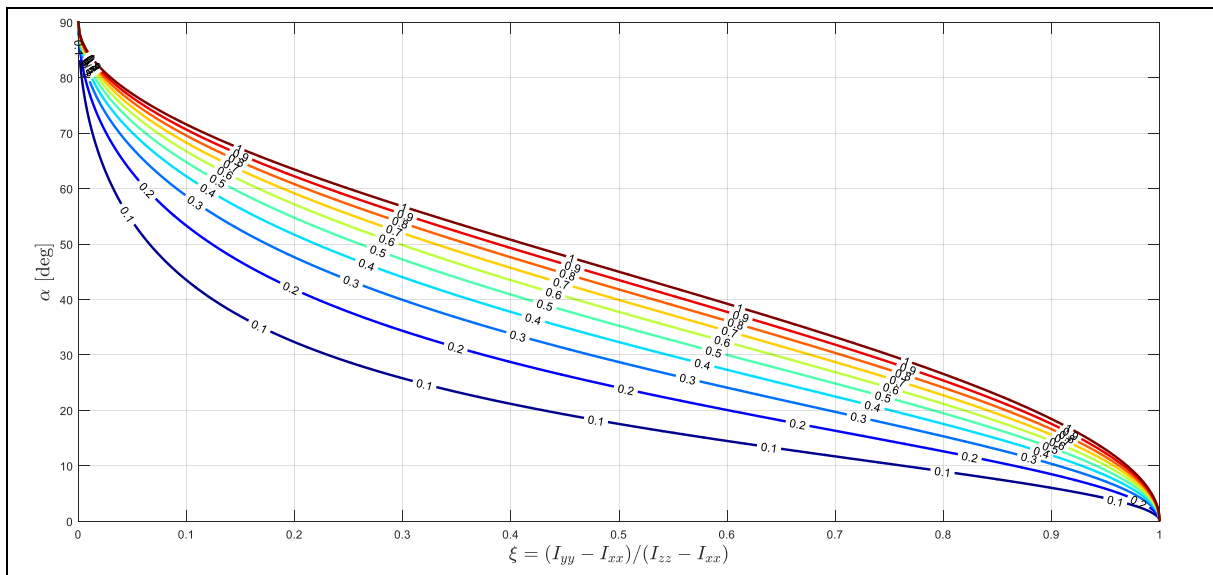


Fig.5: Changes in the angle α due to the variation in ξ for selected values of $\eta=[1:10]/10$.

Kinetic Energy Ellipsoid and Geometric Interpretation of Polhodes

Let us express the kinetic energy of the rotating body in terms of the angular momentum components:

$$\frac{1}{2} I_{xx} \omega_x^2 + \frac{1}{2} I_{yy} \omega_y^2 + \frac{1}{2} I_{zz} \omega_z^2 = \left[\frac{H_x(t)}{\sqrt{2I_{xx}}} \right]^2 + \left[\frac{H_y(t)}{\sqrt{2I_{yy}}} \right]^2 + \left[\frac{H_z(t)}{\sqrt{2I_{zz}}} \right]^2 = K(t) \quad (9)$$

It would be essential, in the context of the “inertial morphing” concept (presented later in the paper), to consider the general case allowing for the principal moments of inertia of the system to change with time:

$$\left[\frac{H_x(t)}{\sqrt{2I_{xx}(t)}} \right]^2 + \left[\frac{H_y(t)}{\sqrt{2I_{yy}(t)}} \right]^2 + \left[\frac{H_z(t)}{\sqrt{2I_{zz}(t)}} \right]^2 = K(t) \quad (10)$$

Being dedicated to the non-dimensional formulation, we divide both sides of this equation by constant $H^2(0)$ and rearrange result in terms of non-dimensional quantities \bar{H}_x , \bar{H}_y and \bar{H}_z :

$$\left[\frac{H_x(t)}{H(0)} \frac{1}{\sqrt{2I_{xx}(t)}} \right]^2 + \left[\frac{H_y(t)}{H(0)} \frac{1}{\sqrt{2I_{yy}(t)}} \right]^2 + \left[\frac{H_z(t)}{H(0)} \frac{1}{\sqrt{2I_{zz}(t)}} \right]^2 = \frac{K(t)}{[H(0)]^2} \quad (11)$$

In view of Eqs (6), this equation can be rewritten in terms of the *non-dimensional* angular momentum components:

$$\left[\frac{\bar{H}_x}{\sqrt{2I_{xx}(t)}} \right]^2 + \left[\frac{\bar{H}_y}{\sqrt{2I_{yy}(t)}} \right]^2 + \left[\frac{\bar{H}_z}{\sqrt{2I_{zz}(t)}} \right]^2 = \frac{K(t)}{[H(0)]^2} \quad (12)$$

Finally, last Eq. (12), can be written in its useful final form, used in this paper, as follows:

$$\left[\frac{\bar{H}_x}{\sqrt{2K(t)I_{xx}(t)}} \frac{H(0)}{H(0)} \right]^2 + \left[\frac{\bar{H}_y}{\sqrt{2K(t)I_{yy}(t)}} \frac{H(0)}{H(0)} \right]^2 + \left[\frac{\bar{H}_z}{\sqrt{2K(t)I_{zz}(t)}} \frac{H(0)}{H(0)} \right]^2 = 1 \quad (13)$$

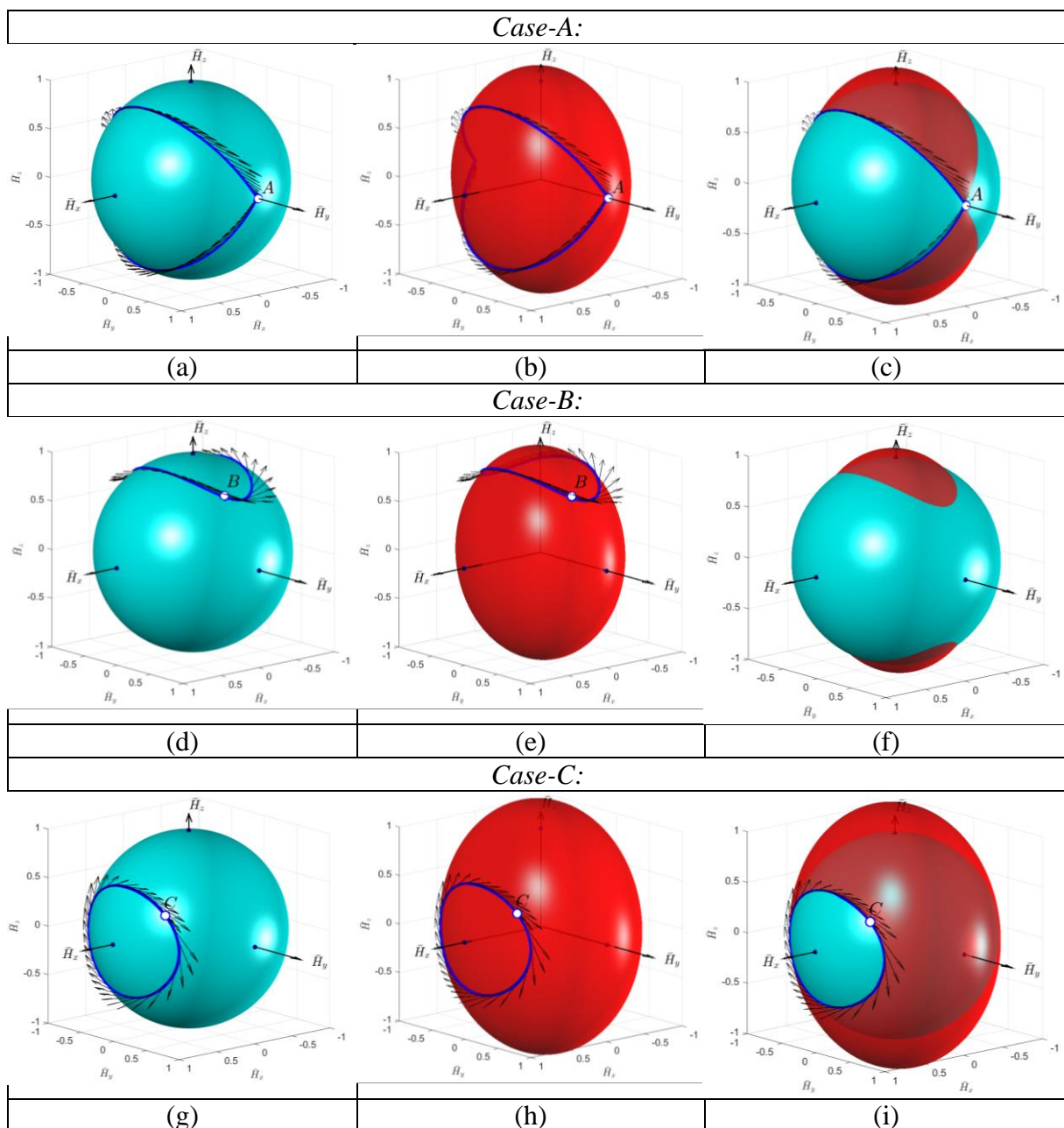


Fig. 6: (a),(d),(g) Angular momentum unit spheres (left column); (b),(e),(h) kinetic energy ellipsoids (middle column) for Cases-A,B,C; (c),(f),(i) Superimposed AMSs and KEEs.

Equation (13) corresponds to the ellipsoid in the \bar{H}_x , \bar{H}_y and \bar{H}_z axis, with the following values of the semi-major axes:

$$\begin{aligned} a_x &= \frac{\sqrt{2K(t) I_{xx}(t)}}{H(0)}; \\ a_y &= \frac{\sqrt{2K(t) I_{yy}(t)}}{H(0)}; \\ a_z &= \frac{\sqrt{2K(t) I_{zz}(t)}}{H(0)} \end{aligned} \tag{14}$$

Let us, in addition to the angular momentum spheres with specific polhodes for the cases A, B and C (Fig.6, left column), plot also corresponding kinetic energies ellipsoids (Fig.6, middle column). Then, combining the surfaces in these two columns, we can see that specific polhodes are, in fact, lines of intersection between corresponding AMSs and KEEs (Fig.6, right column). Utilising conveniences of the non-dimensional notations, we can illustrate influence of the variables ξ and η on the shapes of the kinetic energy ellipsoids and polhodes. Fig.7 presents nine contrast cases for the combinations of $\xi=[0.1, 0.5, 0.9]$ and $\eta=[0.2, 0.5, 0.9]$.

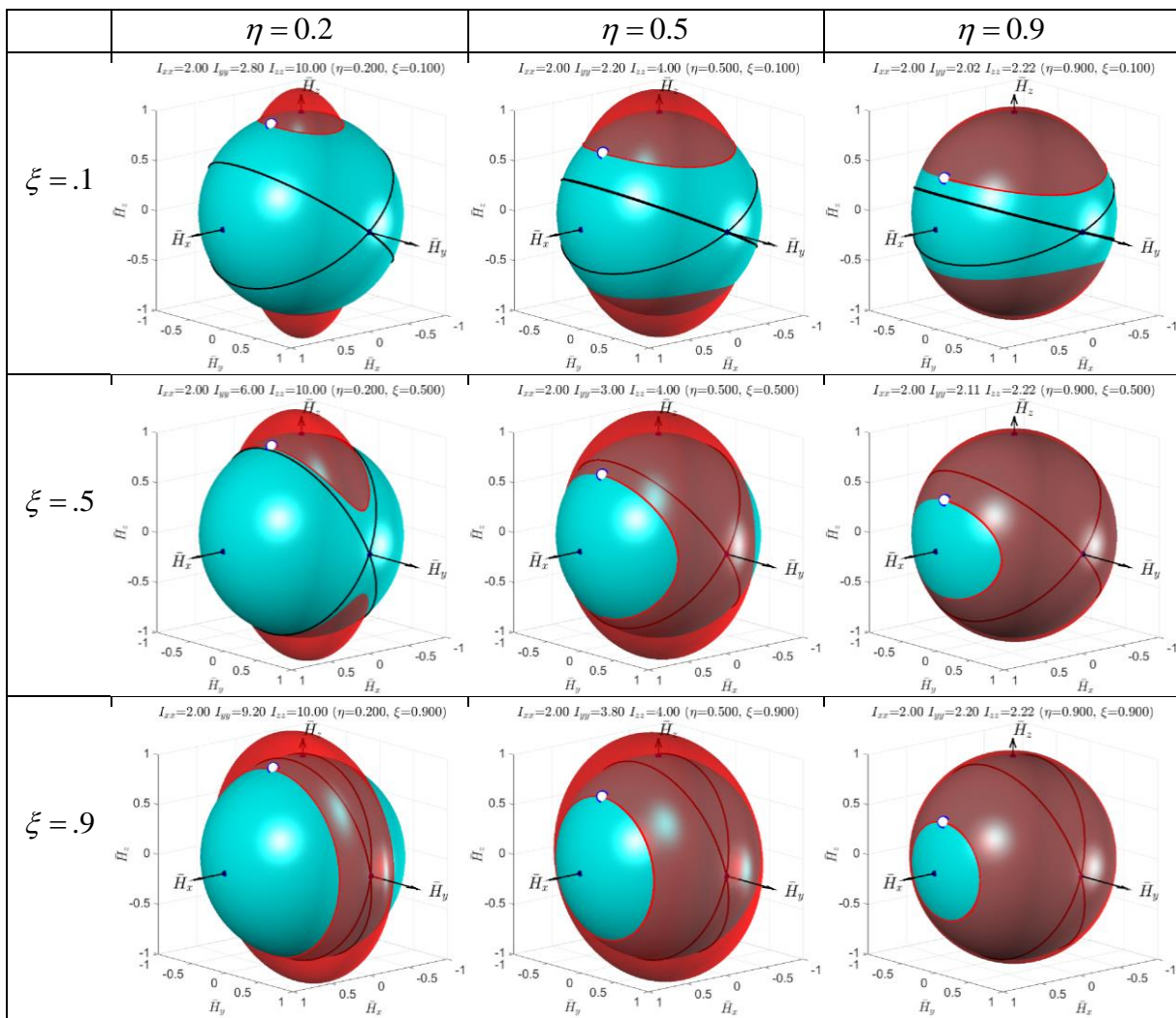


Fig. 7: Contrast cases of simulations of the rotating rigid body with the same initial conditions ($\omega_{x0} = 1$; $\omega_{y0} = 0$; $\omega_{z0} = 1.5$ - all in rad/s) and $I_{xx} = 2 \text{ kg} \times \text{m}^2$, illustrating changes of the shape of the kinetic energy ellipsoid due to the changes in η and ξ .

“Dzhanibekov’s Effect” and Tennis Racquet Theorem

Motion of the spinning rigid body, labelled as Case-A, has a very special significance, as it is related to the so called “Dzhanibekov’s Effect” and “Tennis Racquet Theorem” [5]. Let us present a brief history of this intriguing phenomenon, partially reproduced from [3].



Fig. 8: Dzhanibekov, V.A.: Interview at the “Secret Signs” TV Program, https://youtu.be/dL6Pt1O_gSE

Vladimir Aleksandrovich Dzhanibekov (see Fig.8) is a USSR’s cosmonaut famous with his 5 space flights, making him the Champion in this category. During his fifth space flight, on 25-June-1985, he has discovered a spectacular phenomenon, when a spinning rigid body (being originally a wing nut) in its stable flight suddenly changed its orientation by 180 degrees and continued its flight backwards, simultaneously changing its direction of rotation to opposite! (By the way, wing nuts, shown in Fig. 8 and 9a, are widely used in space for fixing payloads: their shape enables removal of the wingnuts without special tools.)

It was even more amazing to realize, that this pattern of motion has been repeated in the periodic sequence. Similar experiments have been run on-board of the International Space Station. Observing these experiments in space, it could be clearly seen that the spinning object always rotates in the same direction relative to the observation camera (fixed to the "inertial" coordinates frame): that means that in the reference frame of the rotating handle the direction of rotation flips each time its orientation flips.

Surprisingly, the Dzhanibekov’s phenomenon, which initially was perceived by some as counter-intuitive or even mysterious, has been conceptually predicted in 1971 by Beachley [13], however this work for very long time has been left unnoticed and popular, in-depth explanation of the phenomenon has only been very recently presented in the journal publication [5]. “Dzhanibekov’s Effect” has been closely linked to the peculiar behaviour and explanation of the flipped tennis racket, which has received a special name, “tennis racket theorem”.

Explanation of both, “Dzhanibekov’s Effect” and “Tennis Racket Theorem” is based on the great Euler equations, published in their canonical form in 1758 [7].

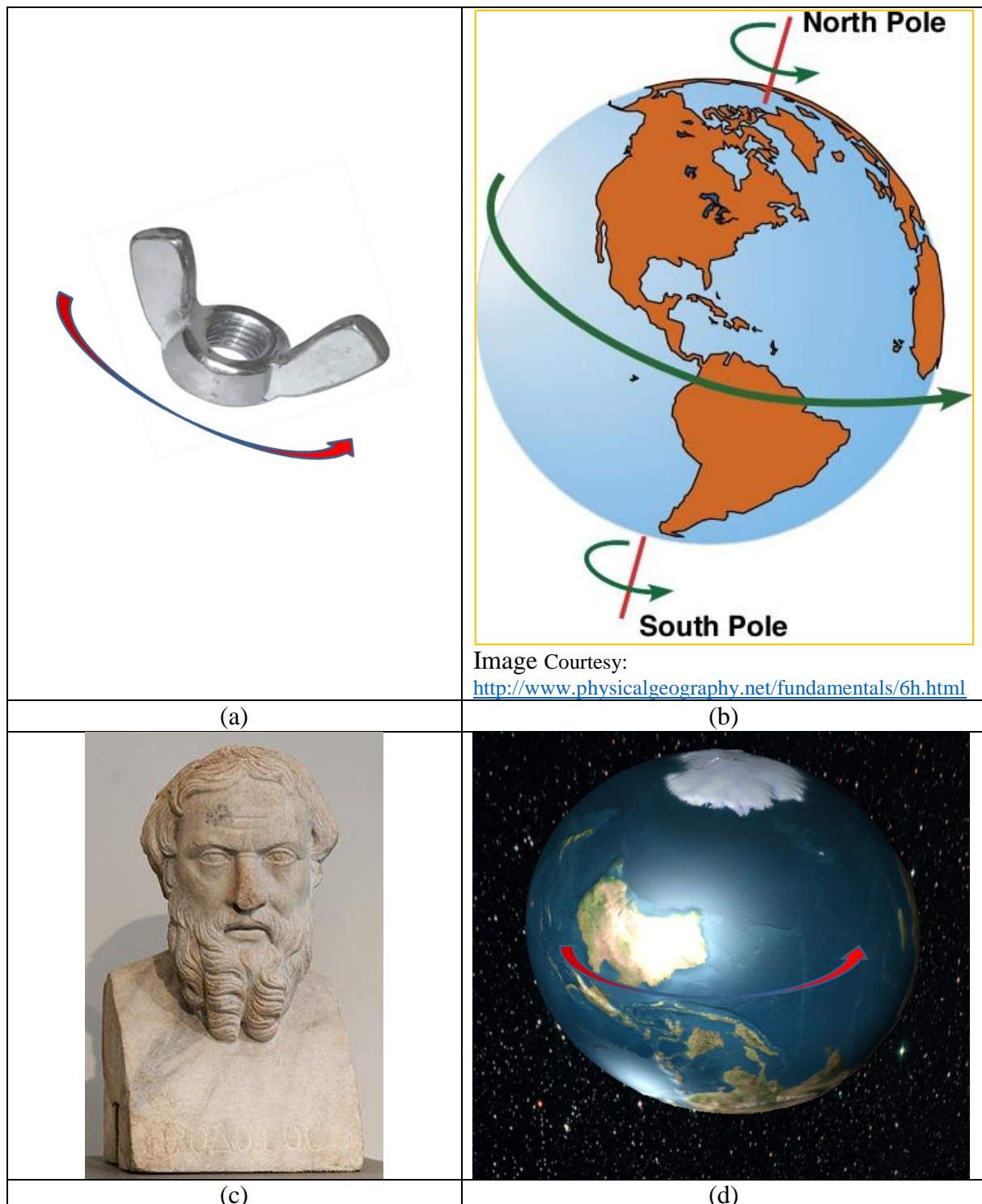


Fig. 9: Is our planet, Earth, flipping similar to the wingnut? (a) simple wingnut; (b) planet Earth; (c) Herodotes, famous Greek historian; (d) imagined “flipped” Earth.

Interestingly, Euler's equations paved the theoretical ground to many scientific manifestations, including Coriolis forces, predicted by Euler, but interpreted to the world many years later by French scientist Gaspard-Gustave de Coriolis in 1835.

Entrancingly, that promotion of the “Dzhanibekov’s Effect” has prompted development of the theories, suggesting that our planet, Earth, is performing periodic flips, similar to the wing nut (see Fig. 9d). Some researchers in the media has suggested that our planet, Earth, having much more substantial properties ($I \sim 8 \times 10^{37} \text{ kg/m}^2$), is performing these flips with much higher period, estimated to be at the order of 12,000 years. There were even some substantiation

presented to justify this statement: firstly, periodicity in the changes in the magnetic field of the Earth, secondly, reference to the ancient Greek historian, Herodotus (lived in the fifth century BC, c. 484–c. 425 BC, see Fig. 8c), and thirdly, references to the religious texts. For example, reference [14] states: “Herodotus wrote that Egyptian priests had told him that four times since Egypt became a kingdom “the Sun rose contrary to his wont; twice he rose where he now sets, and twice he set where he now rises.” The Egyptians had a name for the Sun when it rose in the west, “Re-Horakhty”. And the concept of the Sun rising in the west occurs in both Christian and Muslim literature. There were also accounts of stars reversing the direction of rising, while various texts talk of north becoming south at a time of chaos. This reversal also appears in Greek literature, most notably in the Statesman of Plato.”

Demonstrations of the “Dzhanibekov’s Effect” on-board of the ISS

Due to its simplicity and spectacular nature, the Dzhanibekov’s effect has become one of the most popular educational and scientific experiments on-board of the ISS. It has been reproduced with various rigid body objects and even liquids. Various videos on these experiments, available in the media and on YouTube, are excellent educational resources. For example, influence of the shape of the rigid bodies, thus mass distribution in various rigid bodies, including cylinders, cubes and right rectangular prisms, was demonstrated on board of the ISS by Dan Burbank and Anton Shkaplerov (see Fig.10a), members of the 30-th expedition [15].

American astronaut Kevin Ford (NASA), (34-th expedition) [16] (see Fig.10b) and Japanese astronaut Koichi Wakata (JAXA), (38-th expedition) [17] (see Fig.10c) experimented on-board of the ISS with nothing more complex than pliers. They used this adjustable geometry tool as an object, capable of intriguing spinning, flipping and tumbling in zero gravity.

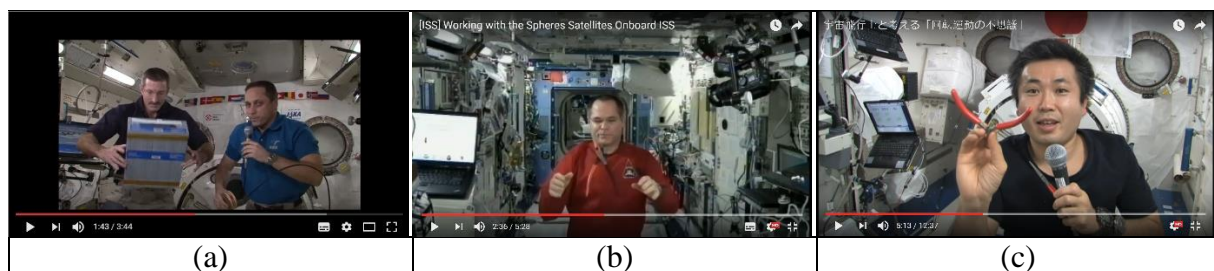


Fig. 10: Demonstrations of the “Dzhanibekov’s Effect” on-board of the ISS.

One of the most fascinating movies is a continuous short-period flipping of the T-handle on-board of the ISS, fairly called as “dancing T-handle” [18] (see Fig.11). This is a wonderful demonstration of the “Dzhanibekov’s Effect”, which very convincingly illustrates instability of rotation of the rigid body with distinct principal moments of inertia, if the main spin is provided about its principal axis, associated with intermediate moment of inertia.

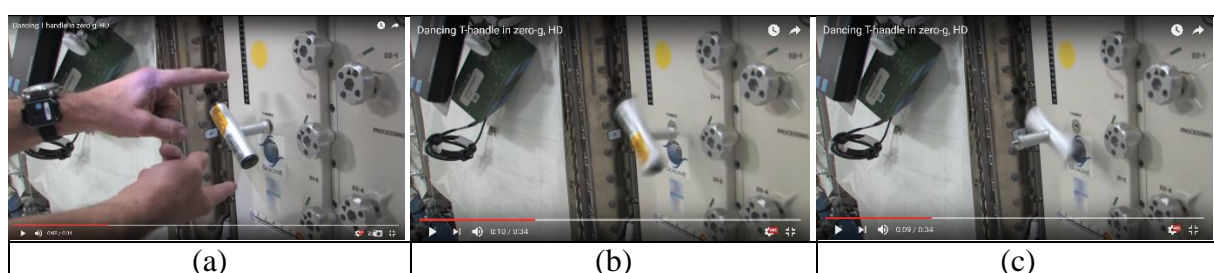


Fig. 11: Dancing T-handle in zero gravity.

All these and other demonstrations can be explained with famous Euler equation. Of course, this is of great interest to be able to explain interesting phenomenon of the flipping spinning systems, however, we noticed new opportunities of controlling these peculiar motions and proposed a method of control, based on the inertial morphing, involving changes of the principal moments of inertia of the system. This concept will be explained later on in the paper. However, before this, let us discuss calculation of the period of the flipping motions in the Dzhanibekov's Effect and Tennis Racquet Theorem demos. We present some interesting results and a relevant extract from our work [3].

Calculation of the Period of the Flipping Motion

We assume, that I_{yy} is intermediate value of the principal moment of inertia. Then the period of the observed unstable motion can be estimated, using Eq. (37.12) in page 154 from the L.D.Landau reference [19]:

$$\text{If } H^2 > 2K_0 I_{yy}, \quad (15)$$

which is equivalent to $a_y < 1$ (see Eq. 12), then

$$T = 4K \sqrt{\frac{I_{xx} I_{yy} I_{zz}}{(I_{zz} - I_{yy})(H^2 - 2K_0 I_{xx})}} \quad (16)$$

$$\text{If } H^2 < 2K_0 I_{yy}, \quad (17)$$

which is equivalent to $a_y > 1$ (see Eq. 12), then

$$T = 4K \sqrt{\frac{I_{xx} I_{yy} I_{zz}}{(I_{xx} - I_{yy})(H^2 - 2K_0 I_{zz})}}, \quad (18)$$

where K is complete elliptic integral of the first kind:

$$K = \int_0^1 \frac{ds}{\sqrt{(1-s^2)(1-k^2 s^2)}} = \int_0^{\pi/2} \frac{du}{\sqrt{1-k^2 \sin^2 u}} \quad (19)$$

As an illustrative example, let us assume the following parameters of the system: $I_{xx} = 0.3$, $I_{zz} = 0.4$ (all in $\text{kg}\cdot\text{m}^2$), with the initial conditions $i\omega_x = 0.1$, $i\omega_y = 15$, $i\omega_z = 0.1$ (all in rad/s). For this case we will use equations (15)-(19) and will illustrate the influence of the intermediate moment of inertia I_{yy} of the system on the period of the unstable flipping motion. Resulting plot is presented in Fig. 12.

The shape of the plot in Fig. 12 is clearly asymmetrical, and could be easily seen by many as counter-intuitive, as there may be a wrongly perceived assumption of the ‘‘symmetrical’’ influence of I_{yy} on period T .

Assuming $I_{xx} = 1$, we can also calculate more generic plot, showing influence of two other principal moments of inertia on the period of the unstable motion. The resultant plot is shown in Fig. 13a, which is also repeated in Fig. 13b and 13c, giving higher resolution for smaller values of T by changing the T -axis limits. This is a very interesting plot, which shows more generic nature of the asymmetry, observed in Fig. 12.

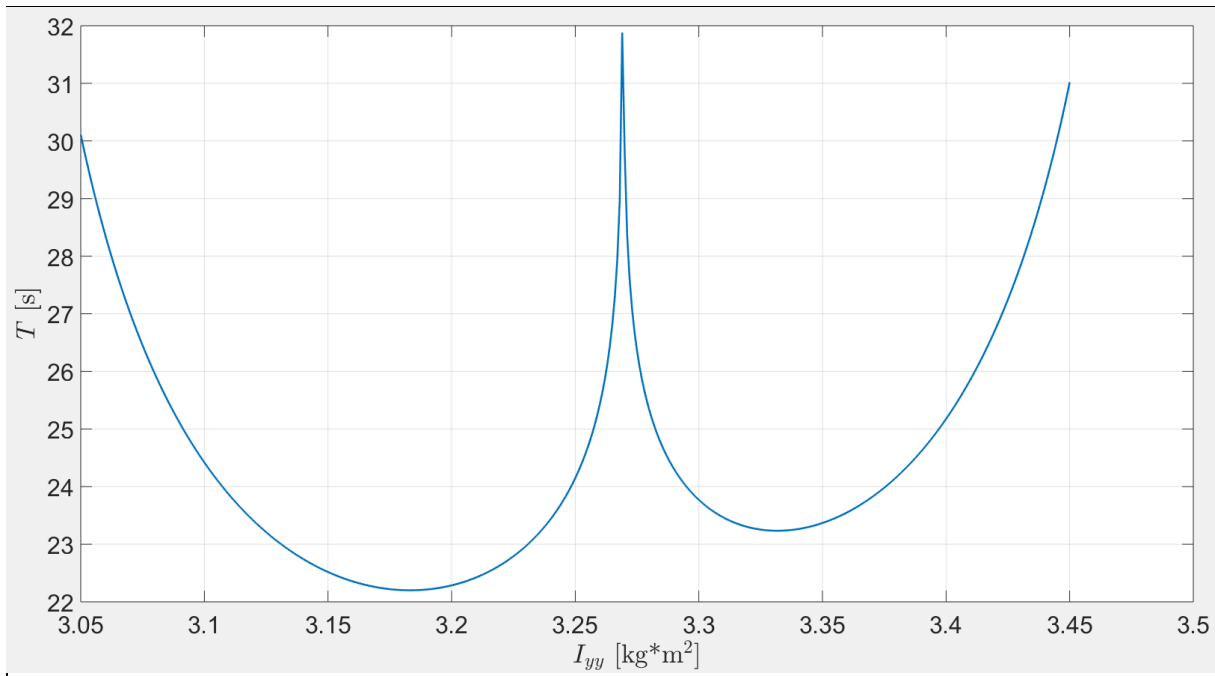


Fig. 12: Period of the unstable flipping motion (“Dzhanibekov’s Effect” case) of the rigid body, as a function of its intermediate moment of inertia I_{yy} .

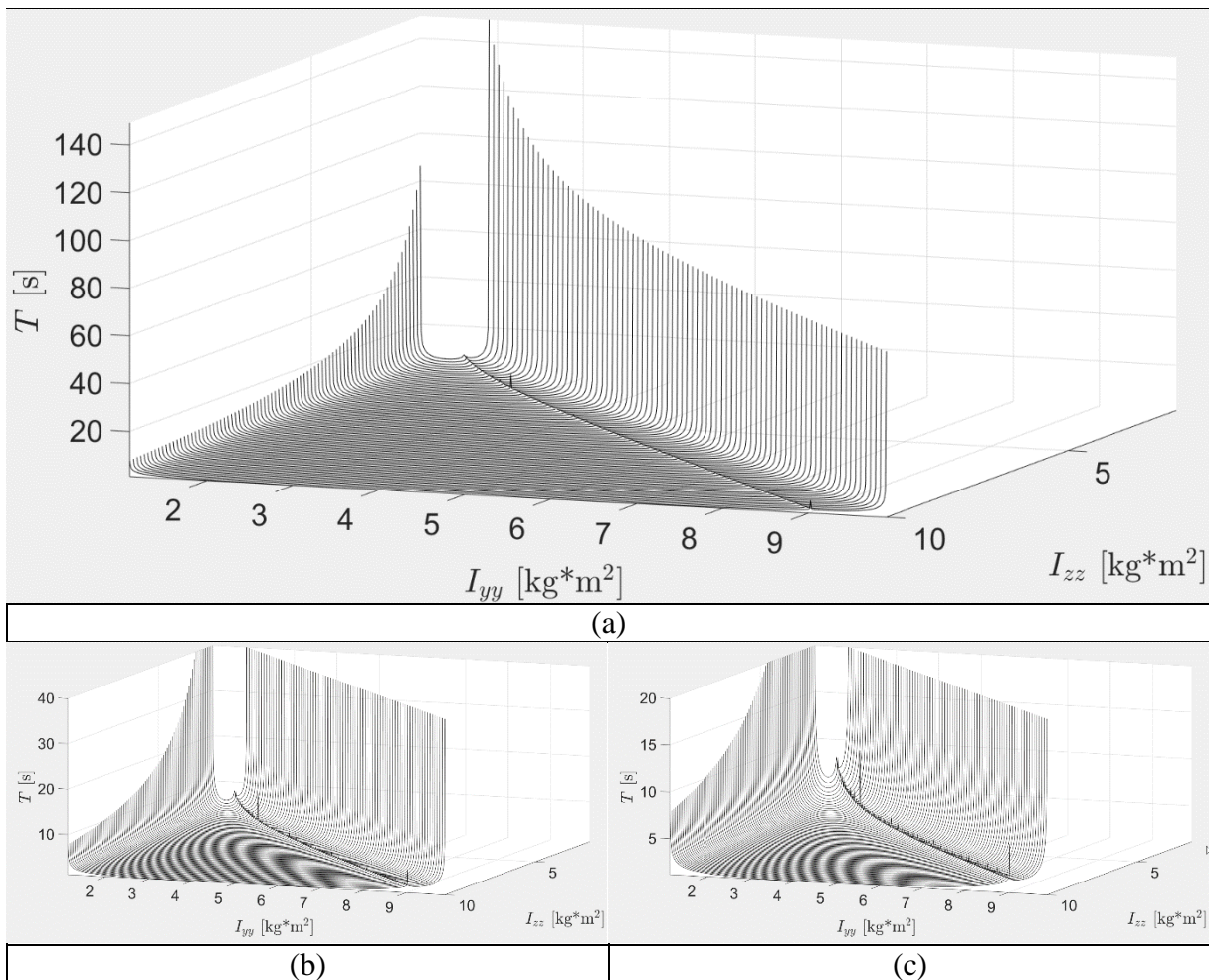


Fig. 13: Period of the unstable flipping motion (“Dzhanibekov’s Effect” case) of the rigid body, as a function of its moments of inertia I_{yy} and I_{zz} : plots (b) and (c) are giving higher resolution along T axis.

Concept of the Inertial Morphing of the Spacecraft

As an enhancement in the control capabilities of the spacecraft, in our previous works [1-4], we proposed a concept of inertial morphing: we showed that using special devices (with, for example moving masses) or other means and/or phenomena, (for example, moving liquids, mass evaporation, solidification, ablation), enabling controlled modifications of the principle moments of inertia characteristics, the attitude dynamics of the spacecraft could be efficiently controlled.

Assume that the spacecraft has morphing capabilities, allowing independent controllable changes of the values of the principal moments of inertia. A basic model of the morphing spacecraft, involving three orthogonal dumbbells, each of which has negligible mass of the rod, connecting two equal concentrated masses at its ends, was considered in [4] and is reproduced in Fig.14.

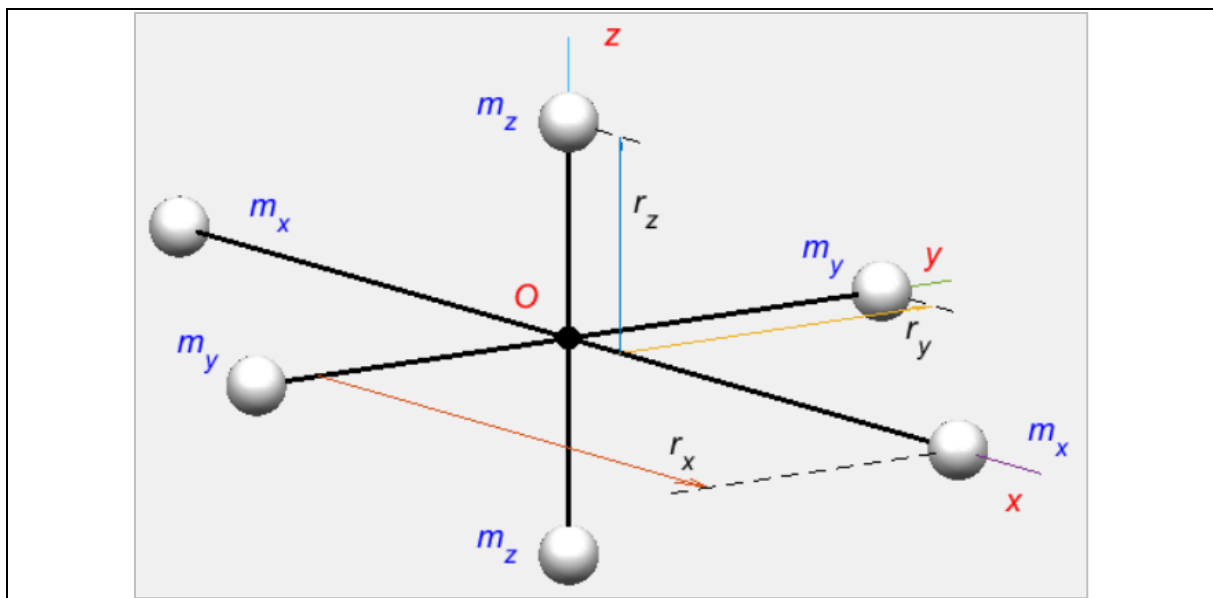


Fig. 14: Six-masses conceptual model of the morphing spacecraft.

Let us also assume, for conceptual simplicity, that three dumbbells are connected at the middle points of their rods, and the corresponding masses m_x , m_y and m_z are located at the distances r_x , r_y and r_z from the axes of rotation x , y and z , as shown in Fig. 14. In the illustrated conceptual design, morphing of the spacecraft is achieved via independent synchronized control of the position coordinates $r_x = r_x(t)$, $r_y = r_y(t)$ and $r_z = r_z(t)$ of the masses m_x , m_y and m_z .

Indeed, changing the distance between three pairs of the masses could be used to achieve *any* values of the principal moments of inertia I_{xx} , I_{yy} and I_{zz} . For achieving this objective, it would be sufficient to move masses to the following radii:

$$r_x = \sqrt{\frac{I_{yy} + I_{zz} - I_{xx}}{4m_x}}; \quad r_y = \sqrt{\frac{I_{zz} + I_{xx} - I_{yy}}{4m_y}}; \quad r_z = \sqrt{\frac{I_{xx} + I_{yy} - I_{zz}}{4m_z}} \quad (20)$$

For simulating the spacecraft systems with morphing capabilities, the Euler Equations must be modified to treat principle moments of inertia not as constants (assumed in the classical Euler equations), bus as *variables*.

$$\begin{bmatrix} \dot{I}_{xx} & 0 & 0 \\ 0 & \dot{I}_{yy} & 0 \\ 0 & 0 & \dot{I}_{zz} \end{bmatrix} \begin{Bmatrix} \omega_x \\ \omega_y \\ \omega_z \end{Bmatrix} + \begin{bmatrix} I_{xx} & 0 & 0 \\ 0 & I_{yy} & 0 \\ 0 & 0 & I_{zz} \end{bmatrix} \begin{Bmatrix} \dot{\omega}_x \\ \dot{\omega}_y \\ \dot{\omega}_z \end{Bmatrix} + \begin{bmatrix} 0 & -\omega_z & \omega_y \\ \omega_z & 0 & -\omega_x \\ -\omega_y & \omega_x & 0 \end{bmatrix} \begin{bmatrix} I_{xx} & 0 & 0 \\ 0 & I_{yy} & 0 \\ 0 & 0 & I_{zz} \end{bmatrix} \begin{Bmatrix} \omega_x \\ \omega_y \\ \omega_z \end{Bmatrix} = \begin{Bmatrix} 0 \\ 0 \\ 0 \end{Bmatrix} \quad (21)$$

These equations can be bundled with quaternions or Euler angles relationships. The version from [4] is presented below:

$$\begin{bmatrix} I_{xx} & 0 & 0 & 0 & 0 & 0 \\ 0 & I_{yy} & 0 & 0 & 0 & 0 \\ 0 & 0 & I_{zz} & 0 & 0 & 0 \\ 0 & 0 & 0 & \sin \theta \sin \phi & \cos \phi & 0 \\ 0 & 0 & 0 & \sin \theta \cos \phi & -\sin \phi & 0 \\ 0 & 0 & 0 & \cos \theta & 0 & 1 \end{bmatrix} \begin{Bmatrix} \dot{\omega}_x \\ \dot{\omega}_y \\ \dot{\omega}_z \\ \dot{\psi} \\ \dot{\theta} \\ \dot{\phi} \end{Bmatrix} = \begin{Bmatrix} (I_{yy} - I_{zz}) \omega_y \omega_z - \dot{I}_{xx} \omega_x \\ (I_{zz} - I_{xx}) \omega_z \omega_x - \dot{I}_{yy} \omega_y \\ (I_{xx} - I_{yy}) \omega_x \omega_y - \dot{I}_{zz} \omega_z \\ \omega_x \\ \omega_y \\ \omega_z \end{Bmatrix} \quad (22)$$

These equations have the following “mass matrix” format:

$$[M(t, \mathbf{x})] \{\dot{\mathbf{x}}\} = \{f(t, \mathbf{x})\} \quad (23)$$

and can be solved numerically, using, for example, ode MATLAB[®] Runge-Kutta solver, with “mass matrix” option.

Basic Demonstration of the Inertial Morphing Capabilities: Stopping Flipping Motion in the Dzhanibekov’s Effect Demo [1]

Let us assume, for the illustration purpose, that $m_x = m_y = m_z = 1$ kg, $I_{xx} = 0.3$ kg*m², $I_{yy} = 0.35$ kg*m², $I_{zz} = 0.4$ kg*m². Then, equations (19) would enable us to determine the exact values of the initial radii r_x , r_y and r_z , compatible with the requirements for the I_{xx} , I_{yy} , I_{zz} values:

$$r_x = 0.2500 \text{ m}; r_y = 0.2958 \text{ m}; r_z = 0.3354 \text{ m}. \quad (23)$$

Note that in our example here I_{yy} has an intermediate value among all principal moments of inertia: $I_{xx} < I_{yy} < I_{zz}$, therefore if the spacecraft is provided with the initial angular velocities $\omega_x = \omega_z = 0.1$ rad/s and $\omega_y = 15$ rad/s, with the prevailing rotation about y body axis, then the spacecraft rotation about this axis would be unstable and classical “Dzhanibekov’s effect” periodic flipping would be observed.

Let us during the “flipping” motion, at the instant, when the angular velocities ω_x and ω_z are close to zeros, rapidly change the moment of inertia I_{yy} to its new value of $f I_{yy} = 0.2$ kg*m².

Then the moment of inertia I_{yy} stops being the intermediate value and the rotation about y body axis would becoming stable, without changes in the direction of ω_y .

It has been demonstrated in [1, 4], that there are two classes of solutions. The new values of the position radii, corresponding to the “solution-1”, can be calculated using Eqs. (19):

$$r_x = 0.1581 \text{ m}; r_y = 0.3536 \text{ m}; r_z = 0.2739 \text{ m}. \quad (24)$$

The spacecraft masses at these radius positions are shown in Fig. 15(a) with dark color.

The flipping motion can be also stopped, using “solution-2”. For the purpose of the illustration of the concept, let us consider rapid increase of the I_{yy} from its initial value of $0.35 \text{ kg}\cdot\text{m}^2$ to its new value of $0.5 \text{ kg}\cdot\text{m}^2$. The new values of the position radii, corresponding to the “solution-2” can be calculated, using Eqs. (20):

$$r_x = 0.3162 \text{ m}; r_y = 0.2236 \text{ m}; r_z = 0.3873 \text{ m}. \tag{24}$$

The spacecraft masses at these radius positions are shown in Fig. 15(b) with dark color.

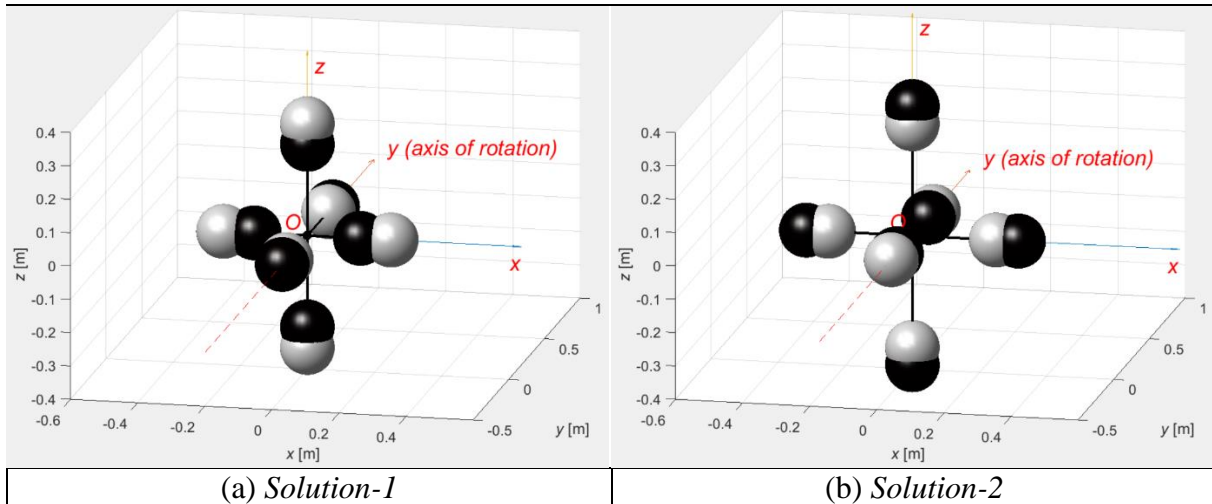


Fig. 15: Graphical representation of solutions for stopping “flipping” motion. White spheres – initial unstable configuration for y main rotation, black spheres – final stable configuration.

Table 1: Numerical Values of the solutions for stopping “flipping” motion.

Solution-1:						
	r_x	r_y	r_z	I_{xx}	I_{yy}	I_{zz}
Initial	0.2500	0.2958	0.3354	0.30	0.35	0.40
Final	0.1581	0.3536	0.2739	0.30	0.20	0.40
Solution-2:						
	r_x	r_y	r_z	I_{xx}	I_{yy}	I_{zz}
Initial	0.2500	0.2958	0.3354	0.30	0.35	0.40
Final	0.3162	0.2236	0.3873	0.30	0.50	0.40

The morphing of the spacecraft from the initially unstable configuration, associated with the “flipping” motion, to its final stable configuration and Solution-1 and 2 are shown in Fig. 15, where masses for the initial configuration are shown in white, whereas the masses for the final configuration are shown in black color. Summary for both solutions is presented in Table 1. It would be important to note, that in the presented cases, it was not obligatory during the morphing of the system and its transition from the “initial” to “final” states to keep both values of I_{xx} and I_{zz} unchanged. However, it was done for purpose to emphasize the role of the I_{yy} in the process of stabilization of the system.

Results of the corresponding numerical simulations of these two solutions are presented in Fig.16-18.

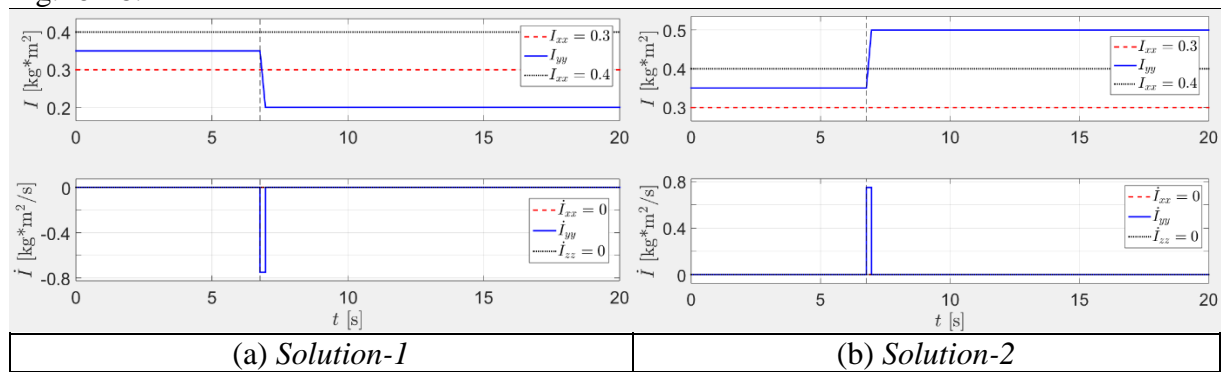


Fig. 16: Graphical representation of solutions for stopping “flipping” motion: Time histories of the required controlled manipulation with the moment of inertia I_{yy} .

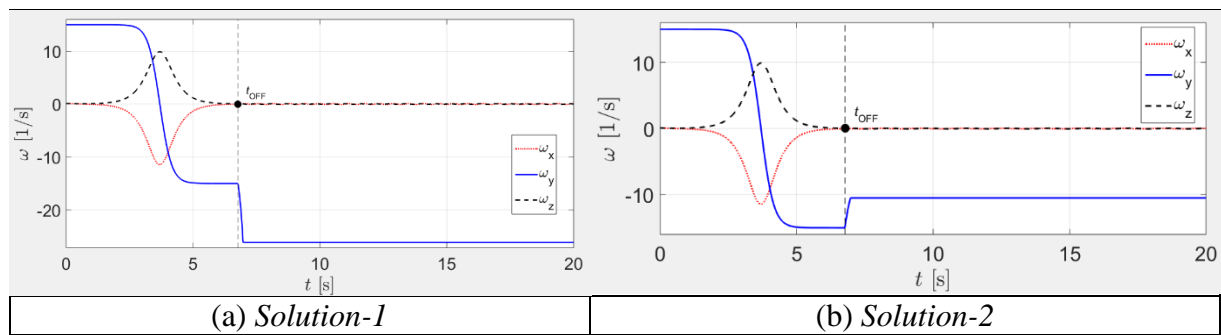


Fig. 17: Graphical representation of solutions for stopping “flipping” motion: Time histories of the $\omega_x, \omega_y, \omega_z$.

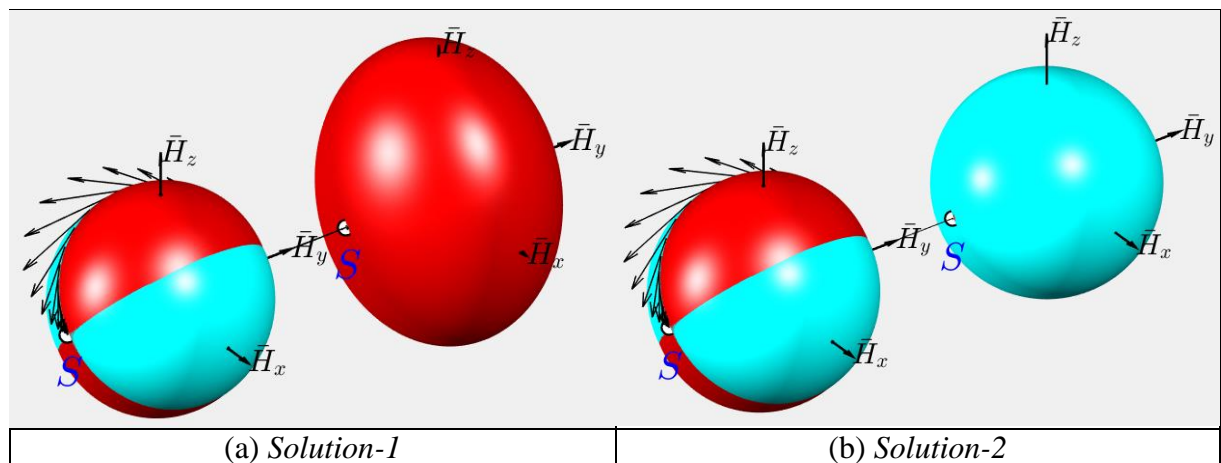


Fig. 18: Graphical interpretation of solutions for stopping “flipping” motion:

It is interesting to note, that with Solution-1, stabilisation of the spinning body is achieved via *expansion* of the kinetic energy ellipsoid, which completely embraces the angular momentum sphere (see Fig. 18a). On the right part of the Fig.18a, both surfaces are just only touching each other at the point S and on the opposite side of the y -axis.

However, with Solution-2, stabilisation of the spinning body is achieved via *shrinking* of the kinetic energy ellipsoid, which becoming completely embraced by the angular momentum sphere (see Fig. 18b). On the right part of the Fig.18b, both surfaces are just only touching each other at the point S and on the opposite side of the y -axis.

Investigating Orientation of the Sides of the Spacecraft, Exposed to the Specific Directions

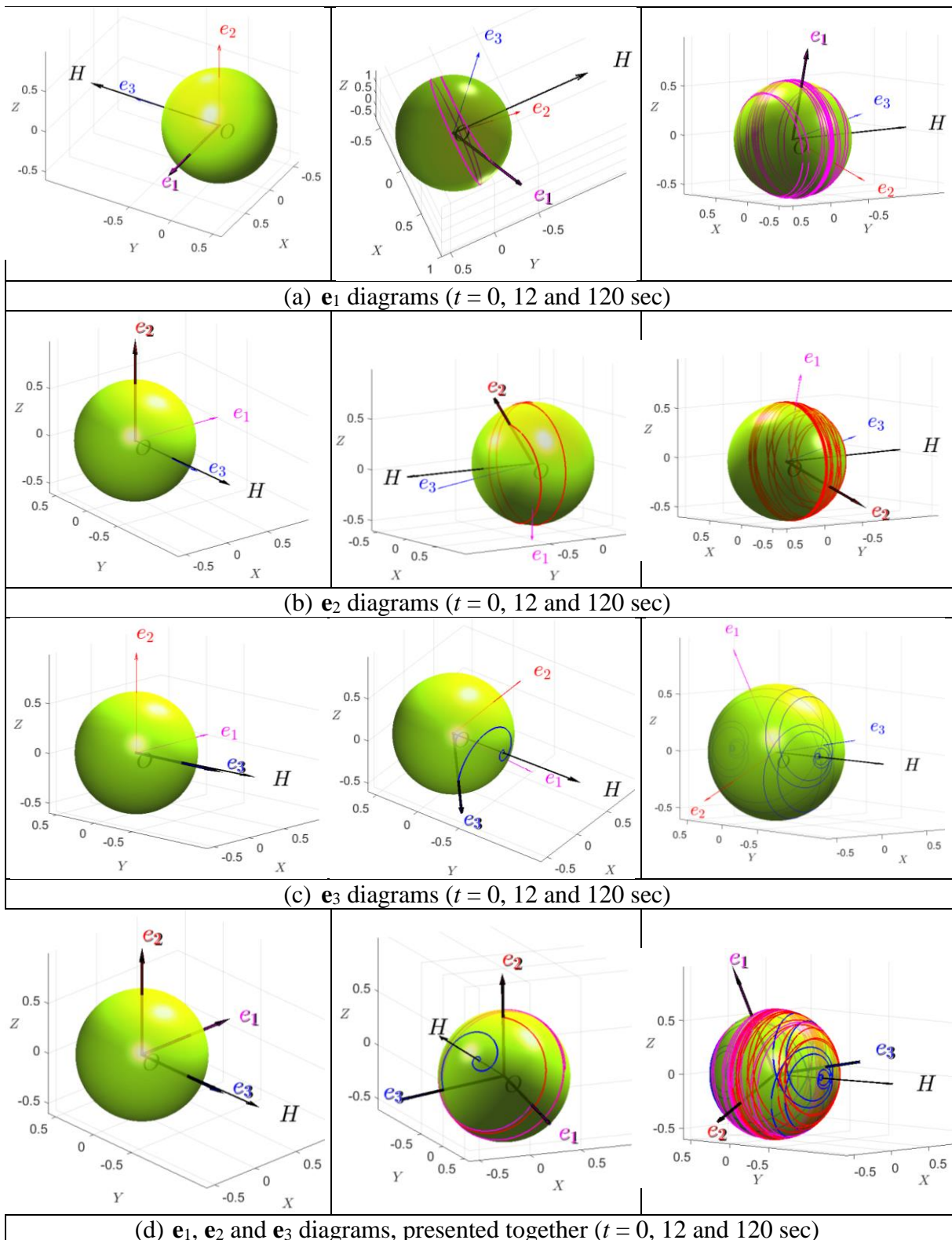


Fig. 19: Lines of intersection of the rotating ors e_1 e_2 and e_3 with the spherical dome (green), fixed in the global axes system XYZ : “ball of wool” lines.

As spacecraft may have directional sensing equipment, attached to the sides, let us explore possible exposure of this equipment to the specified directions of interest. For this purpose let us introduce a semi-transparent green coloured spherical “dome”, embracing the rotating

spacecraft (which, in turn, has its rotating body axes system xyz with unit ors \mathbf{e}_1 , \mathbf{e}_2 and \mathbf{e}_3). We collocate the centre of the dome (point O) with the centre of the mass of the rotating body. However, most significant, we fix the dome in the global coordinates XYZ , so is not rotating with the body and its body axes xyz . Then we consecutively plot lines of intersection of the rotating ors \mathbf{e}_1 , \mathbf{e}_2 and \mathbf{e}_3 with the dome.

For the illustration purposes, let us simulate the motion of the spacecraft with the following parameters: $I_{xx} = 2$, $I_{yy} = 4$, $I_{zz}=3$ (all in $\text{kg}\cdot\text{m}^2$). Let us for $t=0$ align xyz body axes with XYZ global inertial axes as follows: x is aligned with X , y is aligned with Z , z is aligned with $-Y$. If the spacecraft is installed in orbit with initially provided angular velocities $\omega_{x0}=0.01$, $\omega_{y0}=0.01$, $\omega_{z0}=1$ (all in rad/s), the spacecraft starts “flipping” along axis z , being an intermediate axis of inertia (as $I_{xx} < I_{zz} < I_{yy}$).

During this flipping process we trace all intersections of the ors \mathbf{e}_1 , \mathbf{e}_2 and \mathbf{e}_3 with the dome and present them as continuous lines with different colors. Results are shown in Figure 6. It should be noted, that for each of the computer screen snap-shots in this figure, the individual viewpoint was selected for better observation of the simulation results. Selection of the viewpoints could be clearly understood using the vector of the angular momentum \mathbf{H} as a reference, as it is pointing in the same direction in the global coordinates XYZ for all presented snap-shots.

Last image for the \mathbf{e}_2 in the middle row in Fig.19 is remarkably interesting and illustrates our new finding! It shows that y body rotating axis, associated in this example with the maximum moment of inertia, is “drawing” \mathbf{e}_2 intersection lines on the dome only on the hemisphere, bulging towards the angular momentum vector \mathbf{H} (we call it H_+ hemisphere) and is never pointing towards the other hemisphere of the dome (shown as H_- hemisphere in Fig.20). This is valid for the direction of y with positive component of the angular velocity along this direction ($\omega_{y0}>0$). We have run many other various simulations, confirming that it is a general pattern, so the side, perpendicular to the axis with maximum moment of inertia and associated with positive angular velocity component, is never turned away from the vector \mathbf{H} direction!!!

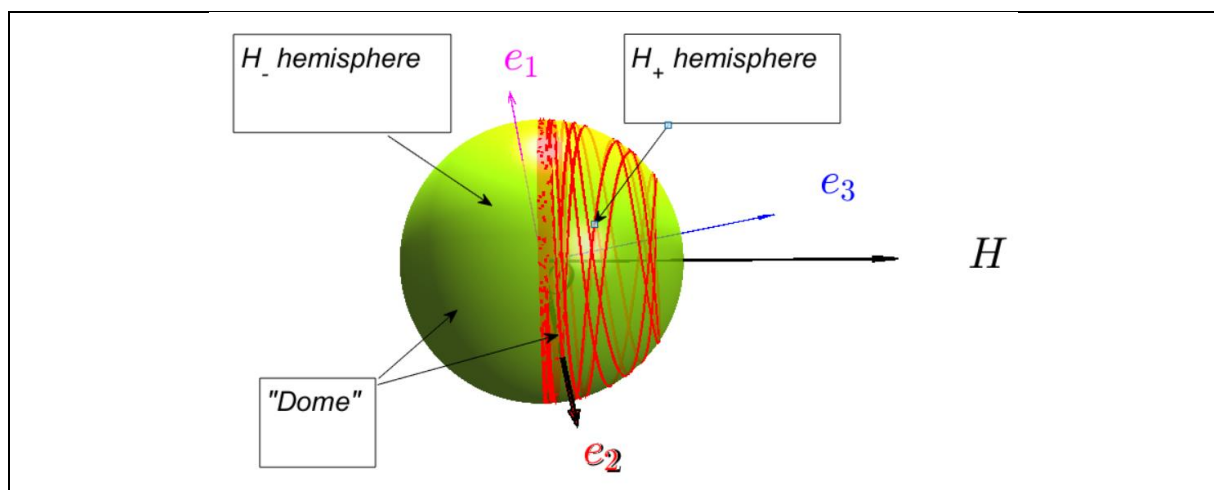


Fig. 20: H_+ and H_- hemispheres of the “dome” ($I_{xx} = 2$, $I_{yy} = 4$, $I_{zz}=3$, all in $\text{kg}\cdot\text{m}^2$; $\omega_x=0.01$, $\omega_y=0.01$, $\omega_z=1$, all in rad/s).

In Fig.19, initially, vector \mathbf{H} is almost aligned with z body axes (which is, in turn, is initially positioned along the $-Y$ global axis), this is because initial values of ω_{x0} and ω_{z0} (and ultimately H_{x0} and H_{z0}) are small compared with ω_{y0} (and ultimately H_{y0}). Therefore, the 2D plane surface, subdividing H_+ and H_- is almost parallel to the XZ plane. H_+ and H_- are also shown in Fig.20.

Let us consider additional contrast case with the following parameters: $I_{xx} = 2$, $I_{yy} = 4$, $I_{zz} = 3$ (all in $\text{kg}\cdot\text{m}^2$) and initial angular velocities $\omega_{x0} = 0.5$, $\omega_{y0} = 0.5$, $\omega_{z0} = 1$ (all in rad/s), which has much more significant initial values of ω_{x0} and ω_{y0} , than in the previous example, hence has large components of H_{x0} and H_{z0} , as compared with H_{y0} . It results in the subdivision of the dome into two parts (H_+ and H_-) by the inclined 2D plane, shown in white in Fig.21a. Results of the intersection lines of the \mathbf{e}_2 ort with the dome are shown in Fig.21a. They somehow resemble “ball of wool” (see Fig.21b), especially with the knitting needles resembling the \mathbf{H} and \mathbf{e}_2 vectors. However, the simulated resulting “ball of wool” lines are “sitting” on one hemisphere only! This hemisphere is on the side of the plane, perpendicular to \mathbf{H} vector (and we will called it H_+ hemisphere). The other side of the hemisphere (H_-) does not have any threads of the “ball of wool”.

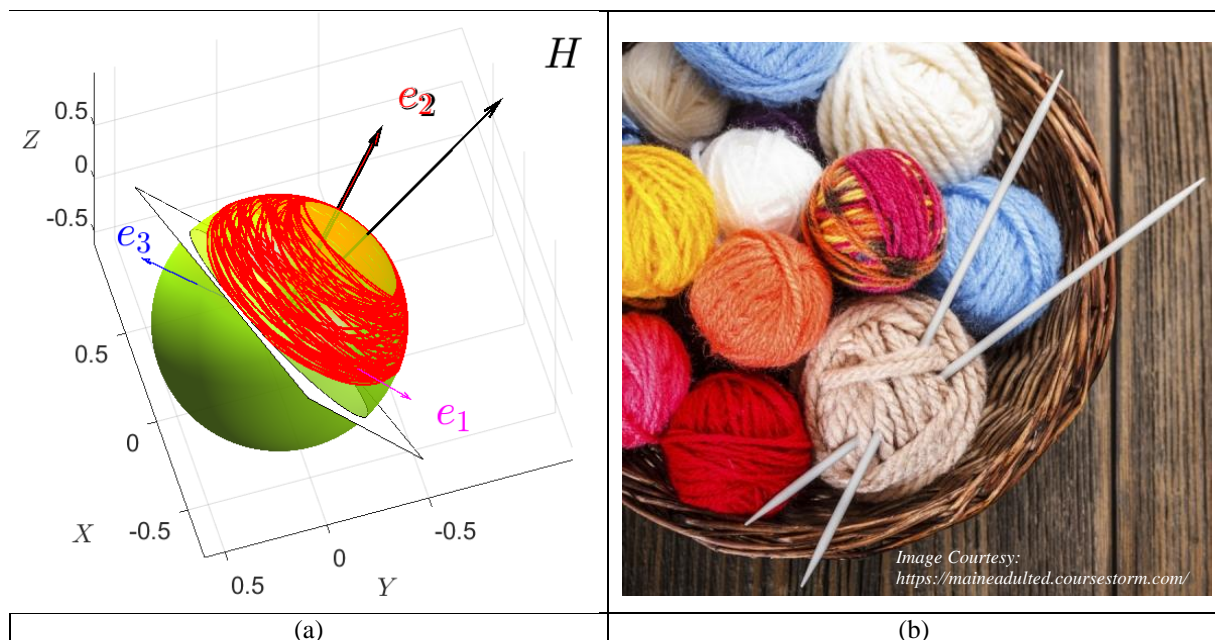


Fig. 21. “Ball of wool” lines: (a) Simulation results for the case $I_{xx} = 2$, $I_{yy} = 4$, $I_{zz} = 3$ (all in $\text{kg}\cdot\text{m}^2$) and initial angular velocities $\omega_{x0} = 0.5$, $\omega_{y0} = 0.5$, $\omega_{z0} = 1$ (all in rad/s), (b) Original “balls of wool”, which prompted the used analogy and terminology.

This discovered new result can be used in the design of various spacecraft missions. For example, in case of the communication mission, if the spacecraft is installed in orbit with predominant rotation about an intermediate axis of inertia, and is carrying an antenna, it should be ensured that the initial direction of the angular momentum vector \mathbf{H} is consistent with the “source”, sensed by antenna, i.e. with H_+ hemisphere facing the “source”, otherwise spacecraft communication would be blanked for all instants of the mission. So, it matters, which side of the spacecraft, perpendicular to the axis with maximum moment of inertia, is selected: one side would be good for utilising antenna, the other side would be inoperable/terminal.

On the same token, in some other cases, when, for example, the spacecraft is subject to directional adhere conditions (heat, radiation, flying debris) it may be advisable to “reinforce” the spacecraft, facing the intended H_- hemisphere, install the spacecraft in orbit with the direction of the initial angular momentum pointing outwards the “danger” and place all sensitive equipment on the side, perpendicular to the axis with maximum moment of inertia and with positive component of the angular velocity along this direction (i.e. “plus” \mathbf{e}_2 in the two previously considered illustration cases).

“Inertial Morphing” In Action: Two-Phase Attitude Dynamics Manoeuvre

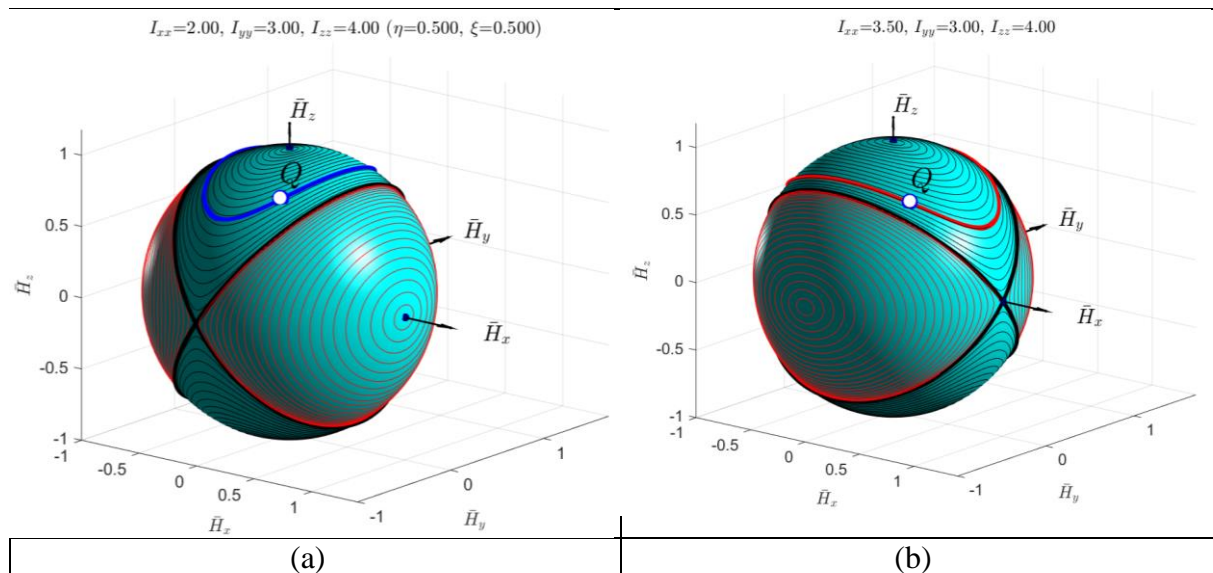


Fig. 22: Non-Dimensional Angular Momentum Spheres with Polhodes and Separatrices and truncated Specific hodographs for (a) Phase-1 (before inertial morphing) conditions: $I_{xx}=2$, $I_{yy}=3$, $I_{zz}=4$, $\omega_{x0}=0.4$, $\omega_{y0}=1$, $\omega_{z0}=0.8$; specific godograph shown with blue line; and (b) Phase-2 (after inertial morphing) conditions: $I_{xx}=3.5$, $I_{yy}=3$, $I_{zz}=4$, $\omega_{xt_Q} = 0.7133$, $\omega_{yt_Q} = -0.7318$, $\omega_{zt_Q} = 0.9016$, $t_Q = 21.5$ s; specific godograph shown with red line

Fig.22(a) shows non-dimensional angular momentum sphere with two separatrices and sets of representative polhodes for the wide range initial conditions. It also shows, as a blue bold line, a specific polhode (or godograph of the $\bar{\mathbf{H}}$ vector) for the Phase-1 conditions: $I_{xx}=2$, $I_{yy}=3$, $I_{zz}=4$, $\omega_{x0}=0.4$, $\omega_{y0}=1$, $\omega_{z0}=0.8$.

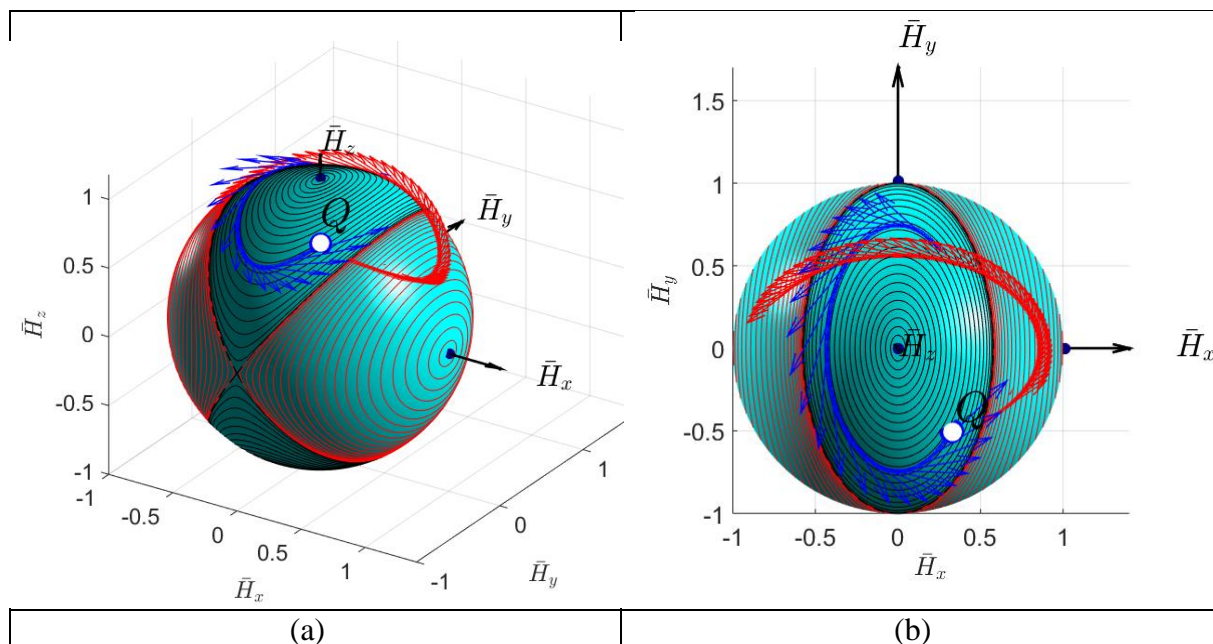


Fig. 23: Illustration of the Transition between Phase-1 and Phase-2 of the inertial morphing of the system: (a) side 3D view; (b) z-axis 2D view.

If the spacecraft possesses with inertial morphing capabilities, then the “switch” to any new inertial properties can be simulated and illustrated graphically. Let assume, for illustration purposes, that the new principal moments of inertia are: $I_{xx}=3.5$, $I_{yy}=3$, $I_{zz}=4$. Then, for the

Phase-2, its own non-dimensional angular momentum sphere with two separatrices and sets of representative polhodes (for the wide range initial conditions) can be also produced (see Fig. 23b). Morphing can be applied at any stage during the execution of Phase-1. For certainly, let assume that the morphing is rapidly applied at $t=21.5$ s instant. Then, the new corresponding angular velocities of the spacecraft could be calculated, using equations (21).

“Inertial Morphing” In Action: Transfer of the Tumbling Motion into Steady Spin about Selected Body Axis (Three-stage stabilisation of the Spacecraft via Inertial Morphing and Unstable Flipping)

Let assume that the spacecraft with given initial values of the moments of inertia ($I_{xx}=2.5$, $I_{yy}=2.4$, $I_{zz}=3.15$) is originally in arbitrary free rotation, involving all three angular velocities, as shown in Fig. 24a.

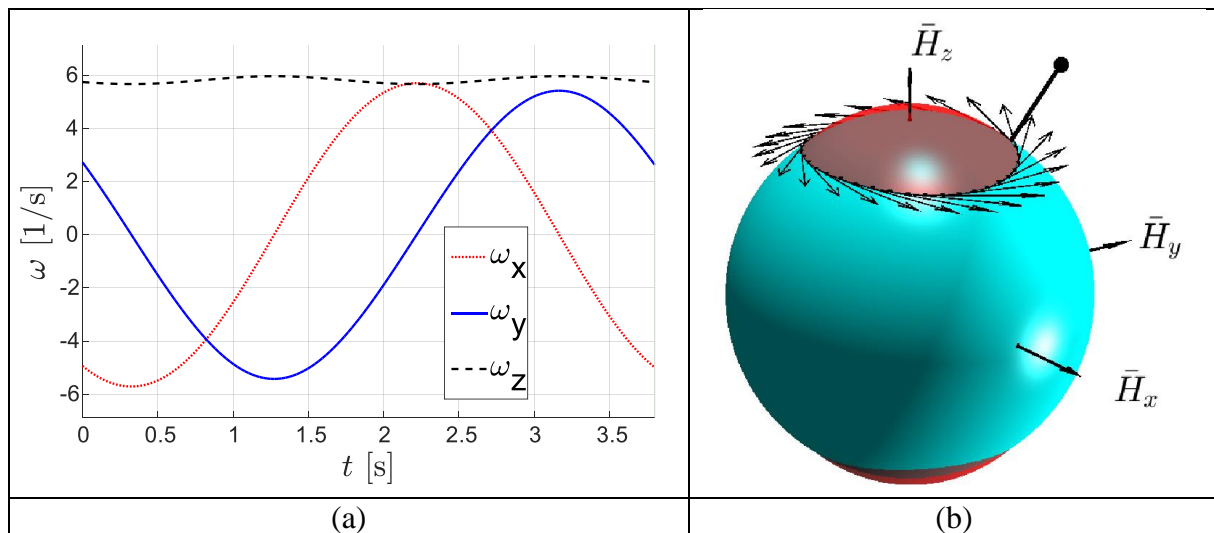


Fig. 24: Illustration of the spacecraft tumbling motion:
 (a) time history of $\omega_x, \omega_y, \omega_z$ - components of its angular velocity vector $\vec{\omega}$,
 (b) graphical interpretation of the motion, using KEE and AMS.

This motion can be visualised, using intersecting kinetic energy ellipsoid and angular momentum sphere, as shown in Fig.24b. The $\bar{\mathbf{H}}$ vector of unit genuine length can not be used for visualization, as its length is equal to one and it would not be seen at any instant, as it would be completely hid by the embracing angular momentum sphere with unit radius. Therefore, for visualisation of the instantaneous orientation of $\bar{\mathbf{H}}$ in the Fig.24b, we use a black line with a dot at its end and extruding beyond the surface of the sphere. The godograph of the $\bar{\mathbf{H}}$ vector is shown with a black line on the surface of the angular momentum sphere, coming strictly along the intersection between the AMS and KEE.

Let us set a task to control rotations of the system, via the changes of the values of its principal moments of inertia. In each case of using flipping mode for escaping from the closed smooth polhoide, we need to apply change to moments of inertia, which could be calculated based on the parameters of the targeted separatrix, using Eqs. (14), (15) or (17).

An example of complete set of morphings, stabilising the system, being initially in the state of tumbling, is illustrated with Fig.25.

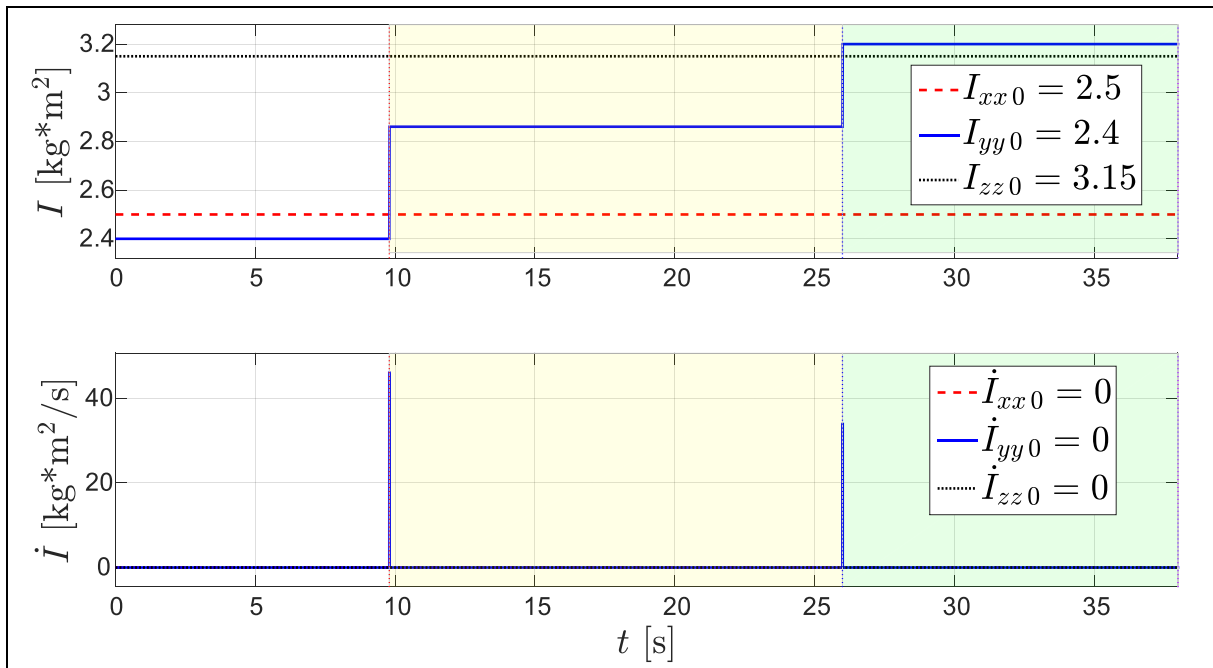


Fig. 25: Three-stage stabilisation of the tumbling spacecraft via morphing: time history of the morphed principal moments of inertia I_x, I_y, I_z .

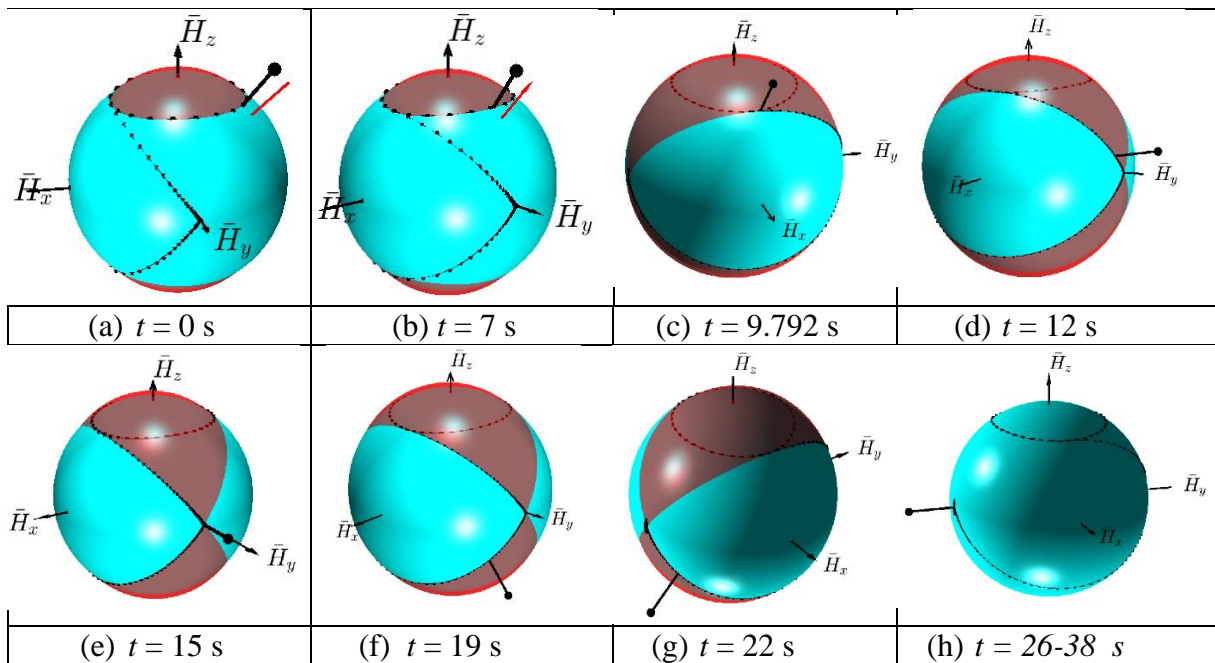


Fig. 26: Critical instances of spacecraft stabilisation: (a) Start of the simulation; (b) Initially, hodograph is “circling” around z axis, (c) Stage-1 ends, transition to “flipping” is initiated, $t=9.792$ s; (d) approach to the saddle point-1, $t=12$ s; (e) near the saddle point-1 (possible “parking” or stabilisation point), $t=15$ s (f) passing saddle point-1, $t=19$ s; (g) approach to the saddle point-2, $t=22$ s; (h) stage-2 ends and third stage starts at $t=26$ s, parking at the stable “saddle point-2 attractor” is activated, stabilisation is completed.

Fig. 25 explains the sequence and nature of the inertial changes, deliberately applied to the system. Fig.26 gives consecutive snap-shots from the simulation process, illustrating changes of the kinetic energy ellipsoid and polhodes - resultant feasible trajectories for the angular momentum vector.

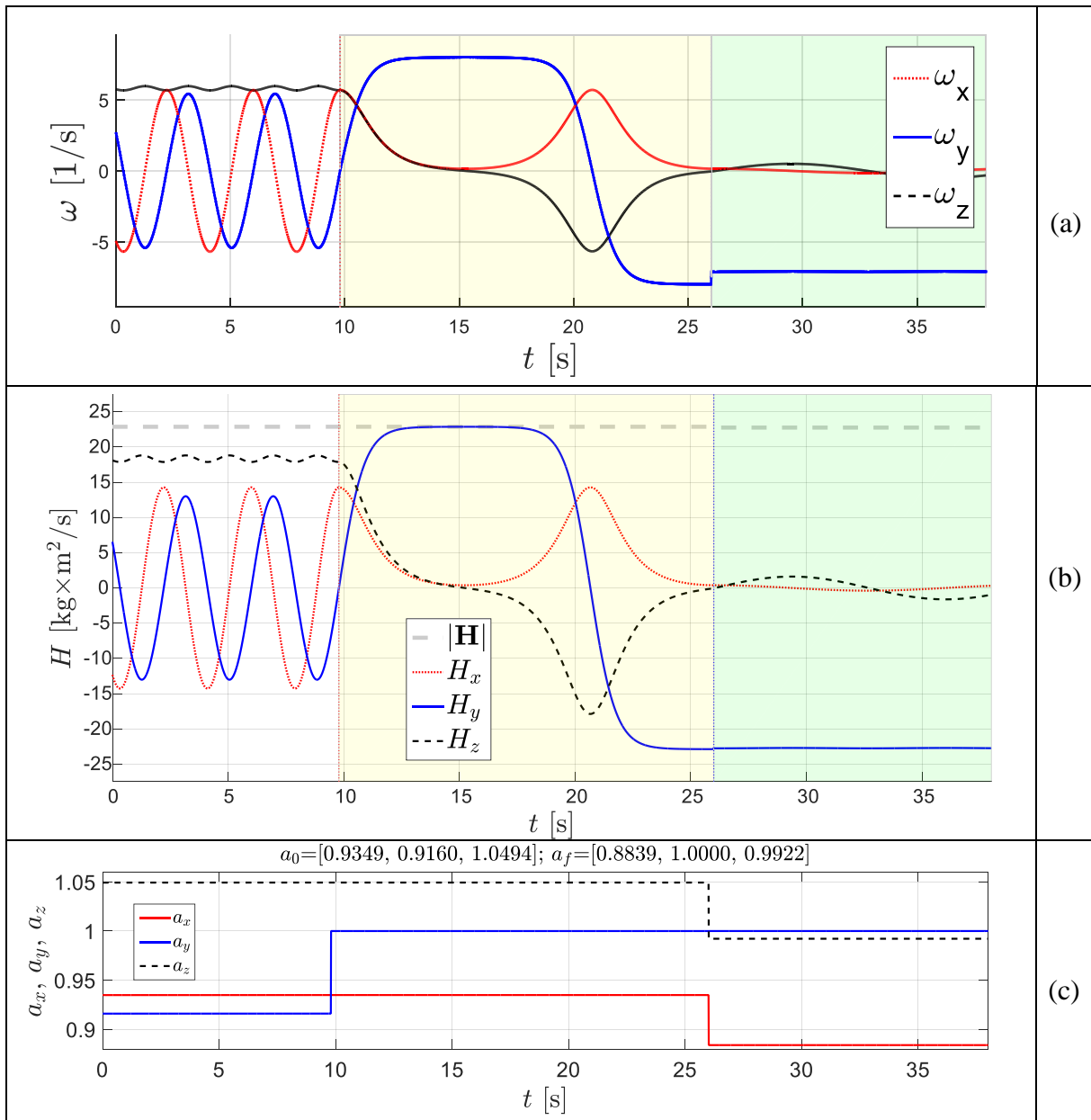


Fig. 27: Time histories of the (a) ω_x , ω_y , ω_z ; (b) H_{total} , H_x , H_y , H_z and (c) a_x , a_y and a_z during two-stage stabilisation of the tumbling spacecraft via morphing.

It is interesting to observe, that at the initial stage of the motion of the system, its e_2 body axes orbit is “drawing” a pretty spread trajectory on the “dome” (Fig. 28a). However, after stabilization is completed, this trajectory is essentially reduced to the point (Fig. 28b). Also, at the last stage of the simulation, trajectories for e_1 and e_3 are very close to the equatorial plane, which confirms that the stabilized motion is close to the rotation of the body along the direction of the angular momentum vector. The feature of the example is: the final direction of the y body axes system, selected for stabilization in this example, is opposite to the direction of \mathbf{H} . If the goal of stabilization was to have them both aligned, then third stage should be activated at instant close to 15 s, as evidenced by the Fig. 27b.

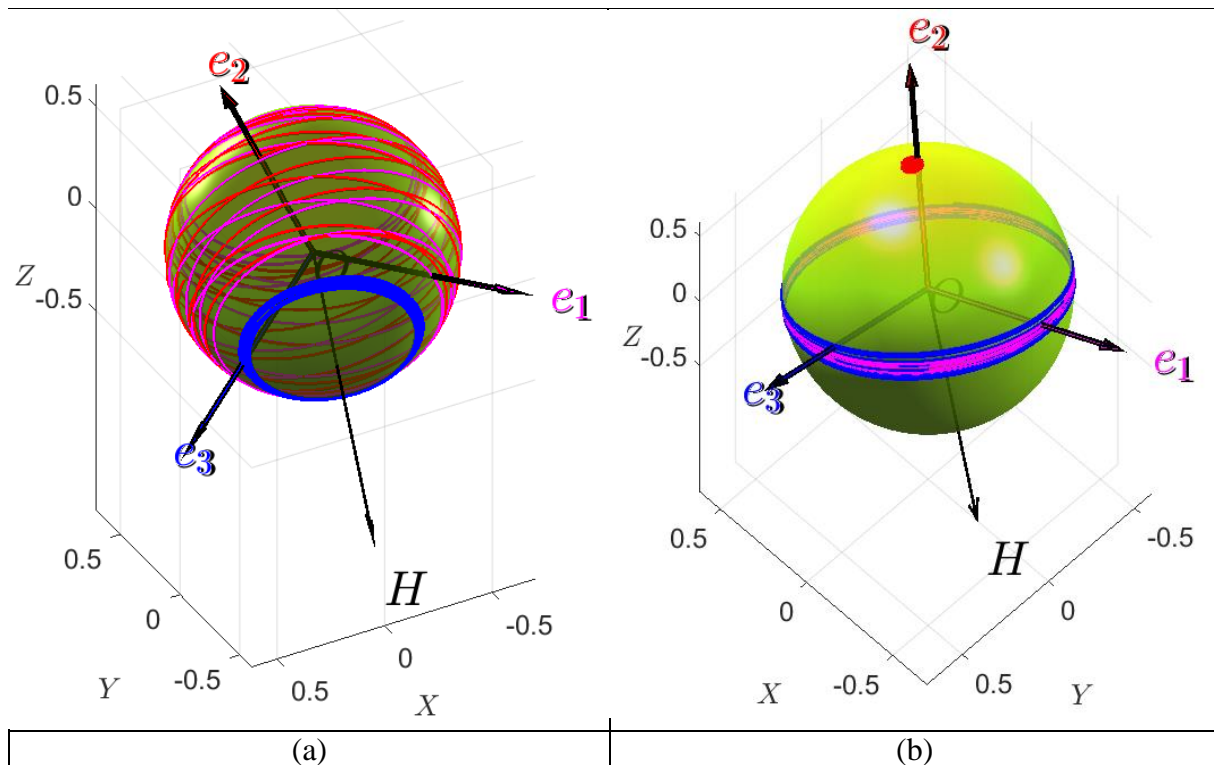


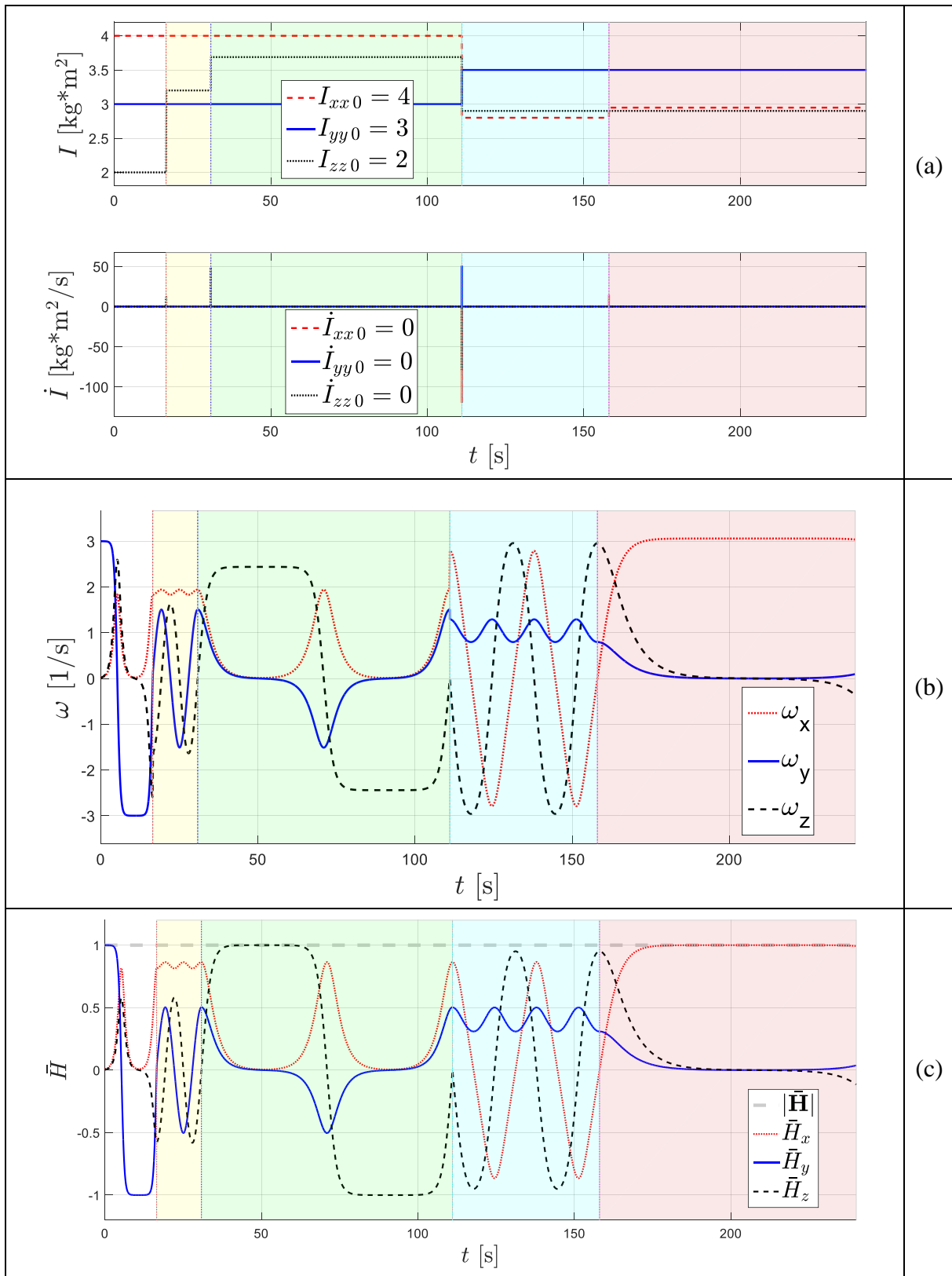
Fig. 28: “Balls of wool” for : (a) the first stage of spacecraft motion with tumbling/coning ($t=0 \div 9.792$ s); (b) last stage of stabilisation of the spacecraft ($t=26 \div 38$ s) with e_1 , e_2 and e_3 intersection lines with the “dome”.

Combined Multi-Phase Demo: Consecutive “Parade” of all Three Orthogonal Inversions, Associated With x , y and z Body Axes

In order to demonstrate capability of the proposed method, in Fig.29 we present results for a single simulation case, during which the spinning body is “reconfigured” four times. The carefully selected scenario for the applied inertial morphing (changes in the system, leading to the change of the values of the principal moments of inertia) enables to achieve the following:

- (1) Established flipping motion along y axis (with possibility for y inversion), distinguished with a white background in Fig.29;
- (2) Established flipping motion along z axis (with possibility for z inversion), distinguished with green background in Fig.29;
- (3) Established flipping motion along x axis (with possibility for x inversion) distinguished with pink background in Fig.29.

So, it has been demonstrated that the predominant spin can be consecutively passed on to any of the body axis with multiple possibilities for inversion at any stage of the stabilised motion and then stabilisation of the desirable orientation. In other words, if the object had a cube shape, based on this example, it was possible to perform transition of the spinning motion of the cube, allowing exposure of each of its six faces to the direction of the initial angular momentum vector. We call this compound demo case “all-axes inversion parade”.



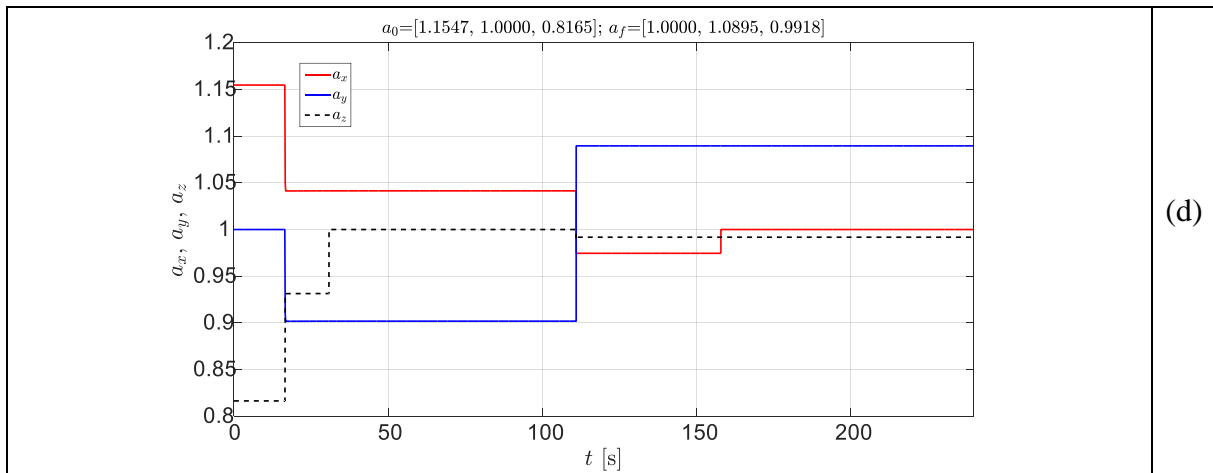


Fig. 29: Time history of the (a) I_x, I_y, I_z ; (b) $\omega_x, \omega_y, \omega_z$ and (c) H_{total}, H_x, H_y, H_z (d) a_x, a_y and a_z during four-stage “all-axes inversion parade”.

Enhancement of the Reorientation and Change of the Spin Axis Using Reaction Wheels

For completeness of this paper, we need to mention another powerful aspect of further enhancement of the spinning spacecraft attitude control capabilities: adding one or a set of moment reaction wheels, which are often used on various space systems [20].

Differential equations of motion of the spacecraft, equipped with wheels, could be presented as follows:

$$\begin{bmatrix} I_{xx} & 0 & 0 & 0 & 0 & 0 \\ 0 & I_{yy} & 0 & 0 & 0 & 0 \\ 0 & 0 & I_{zz} & 0 & 0 & 0 \\ 0 & 0 & 0 & \sin \theta \sin \phi & \cos \phi & 0 \\ 0 & 0 & 0 & \sin \theta \cos \phi & -\sin \phi & 0 \\ 0 & 0 & 0 & \cos \theta & 0 & 1 \end{bmatrix} \begin{bmatrix} \dot{\omega}_x \\ \dot{\omega}_y \\ \dot{\omega}_z \\ \dot{\psi} \\ \dot{\theta} \\ \dot{\phi} \end{bmatrix} = \begin{bmatrix} (I_{yy} - I_{zz}) \omega_y \omega_z - \dot{I}_{xx} \omega_x \\ (I_{zz} - I_{xx}) \omega_z \omega_x - \dot{I}_{yy} \omega_y \\ (I_{xx} - I_{yy}) \omega_x \omega_y - \dot{I}_{zz} \omega_z \\ \omega_x \\ \omega_y \\ \omega_z \end{bmatrix} - \begin{bmatrix} n_{\omega_1} + \omega_2 l_3 - \omega_3 l_2 \\ n_{\omega_2} + \omega_3 l_1 - \omega_1 l_3 \\ n_{\omega_3} + \omega_1 l_2 - \omega_2 l_1 \\ 0 \\ 0 \\ 0 \end{bmatrix} \quad (23)$$

Even simple preliminary cases, involving one wheel and not sophisticated wheel’s controls, enabled us to find significant influence of this enhancement on performance of the system. In particular, it was possible to significantly influence the period of inversion, make inversions asymmetrical (see Fig.30), etc. Authors intend to explore these capabilities in more detail in the future works.

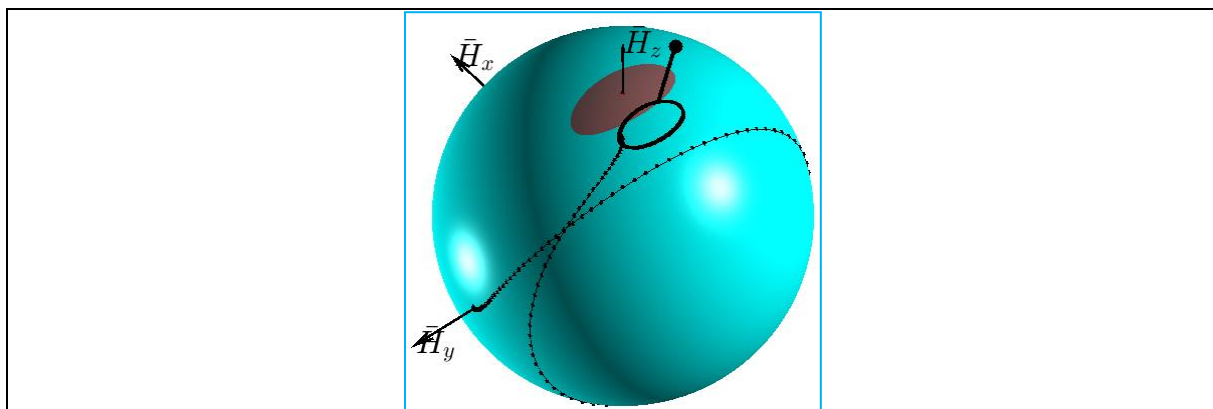


Fig. 30: Shift of stabilisation point, achieved with compounding use of the inertial morphing and reaction wheel.

Conclusions

In this paper we presented methodological platform for enhancing attitude control of the spacecraft, using “inertial morphing”. It is based on the geometrical interpretation of equations of non-linear motion (involving non-dimensionalised angular momentum unit spheres and kinetic energy ellipsoids) and features amazing simplicity, while giving impressive advanced range of tools for preliminary designs of the specific missions. We presented comprehensive non-dimensional mathematical construction/formalization to formulate and solve wide range of attitude dynamics and control problems. Applications of this methodology are vast. We name just a few applications and areas for possible application:

- (a) In particular, “inertial morphing” enables to stop (completely “switch off”) unstable flipping motion of the spinning or tumbling spacecraft, if these motions are undesirable, by translating the motion into the regular spin. On the same token, this methodology enables to initiate (“switch on”) on the spinning spacecraft unstable periodic flipping. Combination of “switching on” and “switching off” capabilities, without using traditional gyroscopic devices, can be used for the inversion of the spacecraft, where the forward/backward flying spacecraft could be easily converted into the backward/forward flying system. Furthermore, this technique can be used for boosting (accelerating) or decelerating spacecraft by only one thruster (i.e. for thruster direction control). It should be stressed out that we demonstrated that there are two classes of possible solutions for “switching off” the flipping motion, presenting multiple alternatives during missions planning/design.
- (b) “Inertial morphing” can be very effective for controlling/changing the frequency of the “flipping” motion within a very wide range. However, we showed that there is a minimum (i.e. low bounding limit) for the period of these oscillations.
- (c) Using “inertial morphing”, we proposed a method of reduction of the compound rotation of the spacecraft into a single stable predominant rotation around one of the body axes. This is achieved via multi-stage morphing. One of the transformation stages employs transition of the system into unstable, “flipping” motion, enabling to transfer the motion into a special type of motion, which could be represented with a polhode, situated close to the separatrix. After this instalment into the separatrix, the final stage of the transition is typically dedicated to conversion unstable motion into the stable. With the capability of this transfer of the spacecraft spin into a single axis spin, aligned with the angular momentum direction, spacecraft essentially could perform three types of inversions, associated with any of three body axis. In order to demonstrate capabilities of the method, we presented “all-axes inversion parade”, during which the spinning system was transitioned through three consecutive stages with inversion, associated with each of the body axes, x , y and z . This is in contrast with the classical Dzhanibekov’s Effect demonstration, where only one axis inversion was possible.
- (d) We investigated attitude orientation of different sides of the spacecraft during various spinning/tumbling scenarios and proposed a simple “ball of wool” method to determine the most advantageous sides of the spacecraft for attaching special equipment, like antennae and/or solar batteries. We discovered, that for the motion, resembling “Dzhanibekov’s Effect” flipping, one side of the prism-shaped spacecraft, perpendicular to the major axis of inertia (named as H_+), would be always sensed from the specified direction, whereas the second side (named as H_-), would never be sensed from the same specified direction. This important finding suggests the strategies for proper placement of the sensitive equipment on the right sides of the spacecraft and for reinforcement of the side, which could be deliberately made exposed to the adverse directional conditions (heat, radiation, flying space debris, asteroid belts, etc.)

It has been also demonstrated that reaction wheel system could further enhance spacecraft capabilities, enabling changes into the angular momentum of the system and full access to the “inertial morphing” strategies.

References

1. Trivailo, P.M., Kojima, H., Discovering Method of Control of the “Dzhanibekov’s Effect” and Proposing its Applications for the Possible Future Space Missions. - Transaction of JSASS (The Japan Society for Aeronautical and Space Sciences), Aerospace Technology Japan, 2019, Vol. 17, No. 1, pp. 72-81. DOI: 10.2322/tastj.17.72.
2. Trivailo, P.M. and Kojima, H., “Augmented Control of Inversion of the Spinning Spacecraft, using Inertial Morphing”, - Paper IAC-18,C2,3,5,x45333, *Proceedings of the 69th International Astronautical Congress (IAC)*, Bremen, Germany, 01-05 October 2018. – 16 pp.
3. Trivailo, P.M. and Kojima, H., “Re-Discovering “Dzhanibekov's Effect” Using Non-Linear Dynamics and Virtual Reality”, - Paper IAC-17,E1,7,10,x41083, *Proceedings of the 68th International Astronautical Congress (IAC)*, Adelaide, Australia, 25-29 September 2017. – IAC, Vol. 17, pp. 11394-11407, - 14 pp.
4. Trivailo, P.M. and Kojima, H., “Utilisation of the “Dzhanibekov’s Effect” for the Possible Future Space Missions”, - Paper ISTS-2017-d-047/ISSFD-2017-047, *Proceedings of the Joint Conference: 31st ISTS, 26th ISSFD & 8th NSAT*, Matsuyama, Japan, 3-9 June 2017. - 10 pp.
5. Murakami, H., Rios, O. and Impelluso, T.J., “A Theoretical and Numerical Study of the Dzhanibekov and Tennis Racket Phenomena”, *Journal Applied Mechanics*, 83, (Sept. 08, 2016), No. 11, 111006 (10 pages). Paper No: JAM-16-1017, doi:10.1115/1.4034318.
6. Portrait of L.Euler. University of Tartu collection, <http://dspace.ut.ee/handle/10062/22581?locale-attribute=en>, (accessed Jan 03, 2019).
7. Euler, L., “Du mouvement de rotation des corps solides autour d’un axe variable,” *Mémoires de l’académie des sciences de Berlin*, Vol. 14, Berlin Academy, Berlin, Germany, 1758, pp. 154-193.
8. The Euler Archive, <http://eulerarchive.maa.org/> (accessed Jan 13, 2017).
9. Feynman R., "Chapter 22: Algebra". *The Feynman Lectures on Physics*, Volume I, June 1970, p. 10.
10. Wells, D., "Are these the most beautiful?". *Mathematical Intelligencer*, 1990, 12 (3): 37–41. doi:10.1007/BF03024015.
11. Wie, B., “*Space Vehicle Dynamics and Control*”, Second Edition, AIAA Education Series, 2008. – 966 pp, doi:10.2514/4.860119.

12. Moler, C., “Tumbling Box ODE. (Cleve’s Corner: Cleve Moler on Mathematics and Computing)”, Posted by Cleve Moler, August 10, 2015. <http://blogs.mathworks.com/cleve/2015/08/10/tumbling-box-ode/> (accessed Nov 04, 2018).
13. Beachley, N. N., “Inversion of Spin-Stabilized Spacecraft by Mass Translation - Some Practical Aspects”, *J. Spacecraft*, 8 (1971), pp. 1078-1080.
14. Theory of the Reversing Earth, <http://www.scientiapress.com/theory-of-the-reversing-earth> (accessed Jan 13, 2019).
15. Shkaplerov, A. and Burbank, D.: Experiments on board of the International Space Station (Expedition #30, 2011). <https://youtu.be/LzVItPwiQyI> (published February 11, 2013; accessed Jan 13, 2019).
16. Wakata, K.: Mysteries of Rotational Movement (Onboard of the ISS, Expedition #38, 2014), JAXA. <https://youtu.be/QhSN2eua14I?t=309> (published Nov 25, 2013; accessed Jan 13, 2019).
17. Ford, K.: Working with the Spheres Satellites Onboard of the ISS (Expedition #34, 2013) <https://youtu.be/dsXOxcDSBLQ?t=108> (published Mar 13, 2013; accessed April 09, 2017).
18. Kawano, D.T., “A Tumbling T-Handle in Space”, Rose-Hulman Institute of Technology. http://rotations.berkeley.edu/?page_id=2472 (accessed Jan 13, 2019).
19. Landau, L.D. and Lifshitz, E.M., *Mechanics*. Vol.1 (In Russian). - 4th ed. Moscow, “Nauka”. 1988. - 216 pp.
20. Terui, F., Kimura, S., Nagai, Y., Yamamoto, H., Yoshihara, K., Yamamoto, T. and Nakasuka, S., Moon Tracking Attitude Control Experiment of a Bias Momentum Micro Satellite “ μ -LabSat”, *Trans. Japan Soc. Aero. Space Sci.*, Vol. 48, No. 159, 2005, pp. 28–33.

\